2006-05-03

Wearable Forehead Pulse Oximetry: Minimization of Motion and Pressure Artifacts

Russell Paul Dresher
Worcester Polytechnic Institute

Wearable Forehead Pulse Oximetry: Minimization of Motion and Pressure Artifacts

A Thesis
Submitted to the Faculty
of the
Worcester Polytechnic Institute
in partial fulfillment of the requirements for the
Degree of Master of Science

By

Russell Dresher
Submitted on: May 3, 2006

Approved:

Professor Yitzhak Mendelson, Ph.D., Major Advisor
Department of Biomedical Engineering

Professor Kristen Billiar, Ph.D., Committee Member
Department of Biomedical Engineering

Michael Leal M.S., Committee Member
Department of Biomedical Engineering

ACKNOWLEDGEMENTS

I wish to extend my deepest gratitude to the following:

Professor Mendelson for his guidance, support, and patience.

My committee members, Professor Billiar and Professor Leal, for their knowledge, constructive criticism, and time spent reviewing my work.

My fiancée Nicole and the rest of my family and friends for their support and patience throughout the past two years.

This research was supported by the U.S. Army Medical Research and Material Command under contract DAMD17-03-2-0006. The views, opinions and/or findings are those of the author and should not be construed as an official Department of the Army position, policy, or decision, unless so designated by other documentation.

ABSTRACT

Although steady progress has been made towards the development of a wearable pulse oximeter to aid in remote physiological status monitoring (RPSM) and triage operations, the ability to extract accurate physiological data from a forehead pulse oximeter during extended periods of activity and in the presence of pressure disturbances acting on the sensor remains a significant challenge. This research was undertaken to assess whether the attachment method used to secure a pulse oximeter sensor affects arterial oxygen saturation (SpO_2) and heart rate (HR) accuracy during motion. Additionally, two sensor housings were prototyped to assess whether isolating the sensor from external pressure disturbances could improve SpO_2 and HR accuracy. The research revealed that measurement accuracy during walking is significantly affected by the choice of an attachment method. Specifically, the research indicated that an elastic band providing a contact pressure of 60 mmHg can result in decreased measurement error and improved reliability. Furthermore, the research validated that the two isolating housings we have investigated improve SpO_2 and HR errors significantly at pressures as high as 1200 mmHg (160 kPa) compared to current commercial housings. This information may be helpful in the design of a more robust pulse oximeter sensor for use in RPSM.

TABLE OF CONTENTS

TABLE OF FIGURES

TABLE OF TABLES

1. INTRODUCTION

Telemedicine is the use of medical information exchanged from one site to another via electronic communications to improve patients' health status [1]. Due to its potential benefits and advances leading to improved electronic and wireless technologies, its use has steadily gained interest in recent years [2] - [5]. Both military and civilian populations could possibly benefit from this technology.

The military could implement this technology for remote monitoring of a soldier's physiological status during combat situations [6]. Since medics may be a significant distance from a soldier, there is a time delay between the instant a soldier is wounded to medic notification of the injury. This delay reduces the chance of medical intervention during the one hour period in which the lives of a majority of critically injured trauma patients can be saved if definitive surgical intervention is provided, otherwise know as the "golden hour" [7], which could mean the difference between life and death. The use of remote physiological status monitoring (RPSM) could notify medics immediately of a casualty, possibly improving the chance of survival during the "golden hour." The off-site acquisition of a soldier's health status has also the potential to save a medic's life. There have been instances where medics died en route to aiding already deceased soldiers.

RPSM could also be used during mass casualty scenarios [3]. In this situation, a simple, multi-variable, physiological sensing device could be attached to multiple casualties after injury. The data from this device could be sent to first responders or hospitals for continuously monitoring the health status of an injured individual. A similar device could be implemented by firefighters, police, and recreational users [8] - [11]. In

these situations, remote monitoring could help to detect early signs of health problems, thus enabling preventive actions to take place as soon as injuries occur.

One potentially attractive approach for implementing RPSM is pulse oximetry. This method is advantageous for assessing a subject's health status for several reasons. First, death results from the lack of oxygen delivery to the heart or brain. Therefore, monitoring of oxygen supply is critical and an appropriate means of monitoring since pulse oximetry measures arterial oxygen saturation (SpO_2) [12]. Another advantage is the ability to measure other vital physiological information from a single compact sensor [13]. Such data could include heart rate (HR), heart rate variability (HRV), and respiration rate (RR).

Despite several advantages, pulse oximetry has yet to be proven effective for RPSM applications. Limiting factors of this technology include the inability to obtain accurate measurements while a subject is physically active or when large pressure disturbances act on the pulse oximeter sensor.

2. BACKGROUND

Oximetry relies on spectrophotometric measurements of changes in blood color to determine oxygen saturation. This method is based on Beer-Lambert's law which relates the concentration of a solute to the intensity of transmitted light through a solution. Knowing the intensity and wavelength of transmitted light, the length of the optical path, and the extinction coefficient (absorbance) of a substance at that wavelength, the concentration of a solute, C, can be determined from:

$$C = \frac{A}{D * E} \tag{1}$$

where, A is the light absorption, D is the optical path length, and E is the extinction coefficient (absorptivity) of the solute. When there is more than one solute, A is the sum of absorbencies for each solute [14].

Spectrophotometric measurements are achieved by the transmission of light at two different wavelengths through tissue bed by light emitting diodes (LEDs) and measuring the light not absorbed by the tissue by a photodetector (PD). This method exploits the fact that deoxyhemoglobin (Hb) has a higher optical extinction in the red region of the light spectrum around 660 nm compared to oxyhemoglobin (HbO_2). In the near-infrared region of the light spectrum around 940 nm, the optical absorption by Hb is lower compared to HbO_2, as shown in Fig. 2.1 [15]. Due to the differences in extinction coefficients, the light absorbed due to HB and HbO_2 can be determined and used to calculate the ratio $A_{660\ nm}/A_{940\ nm}$, which correlates to oxygen saturation [14].

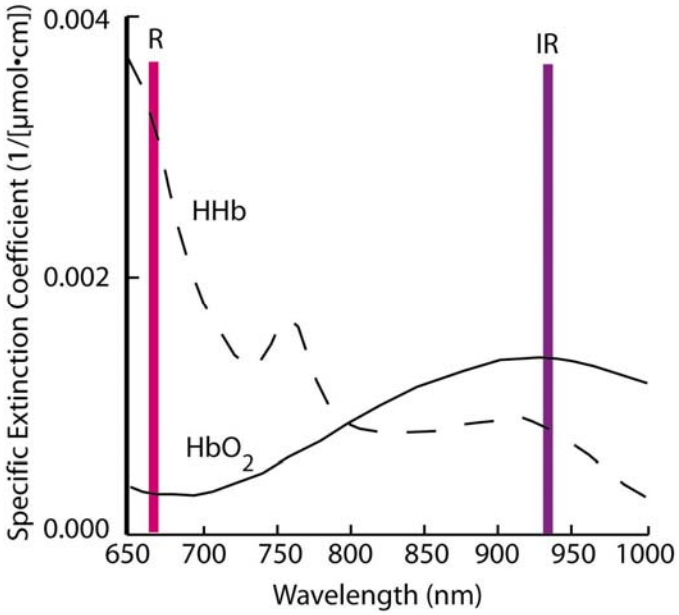

Figure 2.1. Absorptivity spectra of Hb and HbO_2 in the visible and near-infrared wavelength region.

Although other wavelengths provide different extinction coefficients for Hb and HbO_2, as can be seen in Fig. 2.1, selection of 660 nm and 940 nm are preferred. Wavelengths lower than 660 nm result in decreased penetration depths of light and wavelengths greater than 940 nm result in increased light absorption by tissue [14].

Early methods of noninvasive oximetry were not successful as they involved calibration procedures that lead to measurement inaccuracies and lacked reproducibility. These procedures involved squeezing the ear so that transmission of light through the bloodless ear could be measured. This allowed for the measurement of optical absorption due solely to tissue, which served as a baseline measurement. The ear was then decompressed and a second measurement was taken. The optical absorption during this measurement is due to the combination of tissue and blood. The baseline measurement was then subtracted from the second measurement, resulting in the optical absorption of only blood [15], thus allowing for the determination of oxygen saturation.

Pulse oximetry solved the problems associated with earlier approaches by relying on the detection of a photoplethysmographic (PPG) signal produced by arterial blood volume changes associated with periodic contractions and relaxations of the heart [15]. The magnitude of the PPG, shown in Fig. 2.2, is a function of the amount of blood ejected from the heart with each systolic cycle, the optical absorption of blood, absorption by skin and tissue components, and the specific wavelengths used to illuminate the vascular tissue bed [16]. During diastole, blood volume in the vascular bed is decreased, thus increasing the amount of light transmitted or backscattered. This period corresponds to the rising portion of the PPG signal. During systole, when arterial pulsation is at its peak, the volume of blood increases. The increased volume of blood absorbs more light, thus reducing the light intensity measured by the PD. This period corresponds to the decreasing portion of the PPG signal.

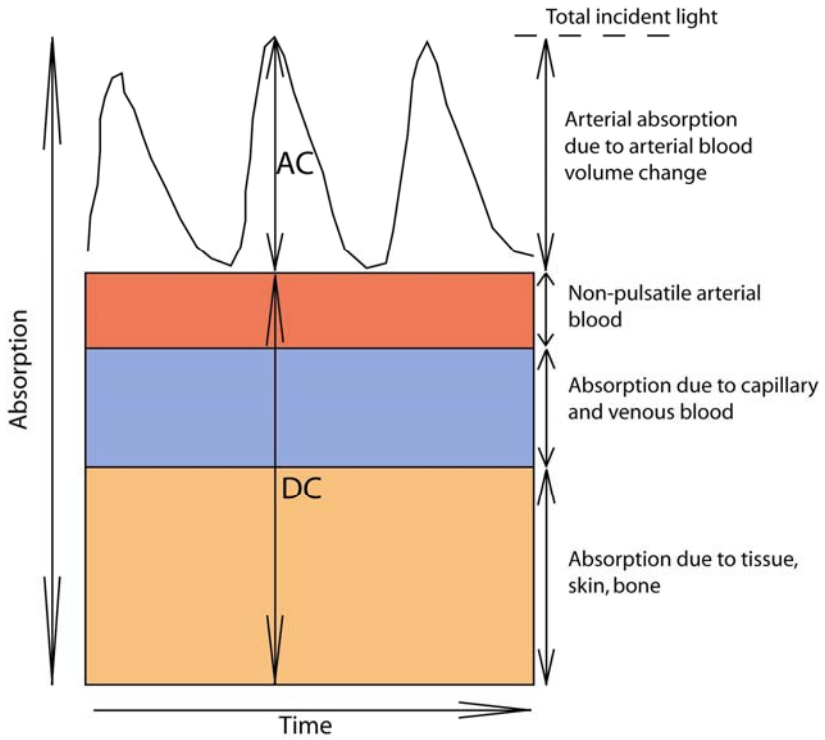

Figure 2.2. Variations in light attenuation by tissue, illustrating the rhythmic effect of arterial pulsation.

2.1. SpO_2 Measurement

The PPG signal is comprised of a non-pulsatile part, referred to as the DC component, and a pulsatile part, the AC component, which are used to calculate an individual's SpO_2. The DC component is due to light absorption by skin, tissue, venous blood, and non-pulsatile arterial blood. The AC component is due to light absorption associated with pulsatile arterial blood flow, as shown in Fig. 2.2. A normalization technique, where the AC component is divided by the DC component, shown below,

$$\frac{R}{IR} = \frac{AC_r / DC_r}{AC_{ir} / DC_{ir}} \tag{2}$$

eliminates the time invariant absorbance due to venous blood or surrounding tissues. This normalization is carried out for both the red (R) and the infrared (IR) wavelengths, as shown in Fig. 2.3. The normalized R/IR results in the so called "ratio of ratios" which pulse oximeter manufactures relate to a set of empirical calibrations specific to their device to obtain SpO_2 [15]. Fig. 2.4 illustrates a typical relationship between SpO_2 and the "ratio of ratios", where a value of 1 for R/IR corresponds to an SpO_2 value of about 85%.

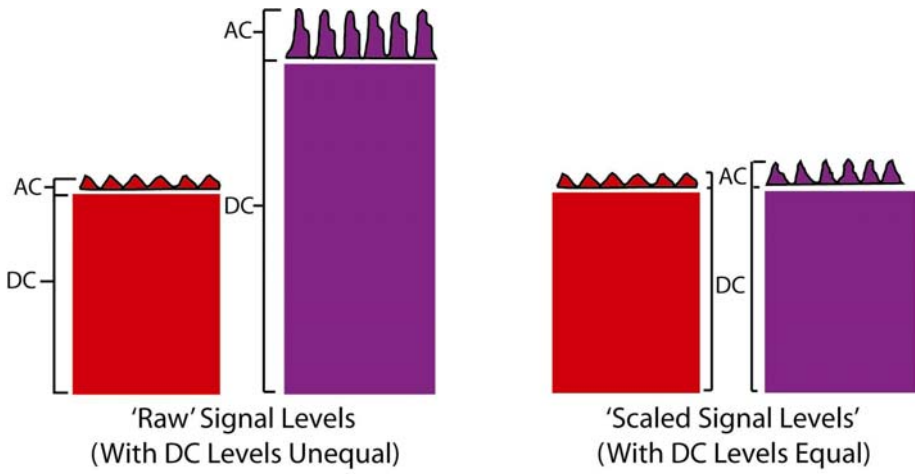

Figure 2.3. Normalization of R and IR wavelengths to eliminate time invariant absorbance effects.

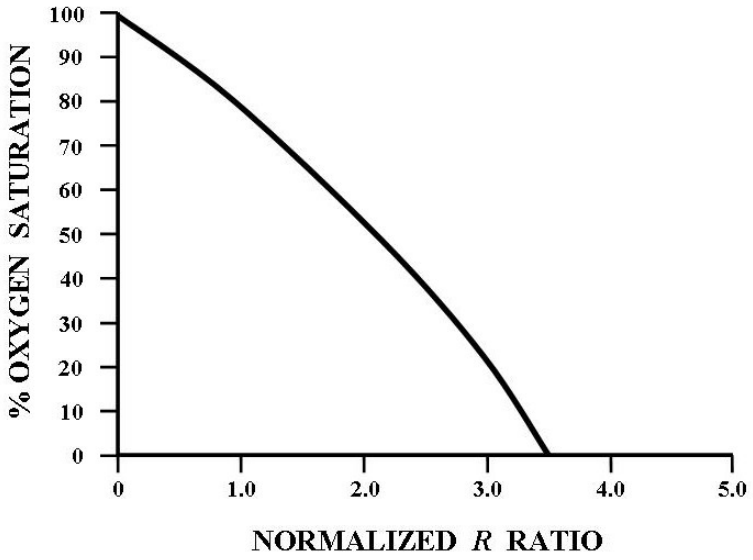

Figure 2.4. Typical empirical relationship relating SpO_2 to the "ratio of ratios." Redrawn from Mendelson [15].

2.2. Heart Rate Measurement

There are two distinct methods used to extract HR from the PPG signal. The first method identifies each individual heart beat peak or cardiac cycle and determines the peak-to-peak time interval, which corresponds to the time to complete one cardiac cycle. Knowing this interval, HR can be easily calculated as the reciprocal of the time interval [17]. The second method relies on the identification of the frequency of cardiac pulsations. A transform, such as the Fourier transform, is used to describe the energy in the frequency components of the PPG waveform, which results in a power spike at the cardiac frequency. HR has shown to be correlated to the frequency where the cardiac spike is observed in the transform [18] - [19].

2.3.Operating Modes of Pulse Oximetry

Pulse oximeters can operate in two different modes, transmission and reflectance. In transmission mode pulse oximetry, the light transmitted through the medium is detected by a PD opposite the LEDs. This method is illustrated in Fig. 2.5. Reflectance mode pulse oximetry, illustrated in Fig. 2.6, consists of the same LEDs but the PD is located on the same planar surface as the LEDs. The PD detects light that is back-scattered or reflected off of the tissue, bones, and blood vessels [20].

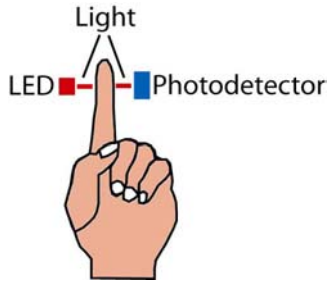

Figure 2.5. LED and PD placement for transmission mode pulse oximetry [21].

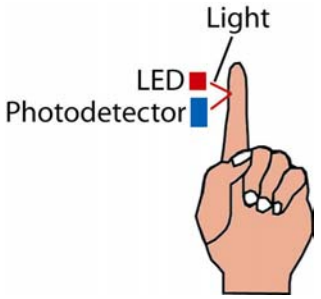

Figure 2.6. LED and PD placement for reflectance mode pulse oximetry [21].

2.4. Transmission Mode Pulse Oximetry and Remote Physiological Monitoring

There are numerous transmission mode pulse oximeters used throughout hospitals and other health care facilities, such as the Avant 4000 manufactured by Nonin Medical Inc [22]. A disadvantage of transmission mode pulse oximetry for use with RPSM applications is the limited measurement sites. To be effective, the sensor must be located somewhere on the body where transmitted light can be readily detected [23]. Locations meeting this criterion include the fingertip, nasal septum, cheek, tongue, ear,

and penis [24] - [28]. Placement on the nasal septum, cheek, tongue, and penis can only be used effectively during anesthesia [29].

Placement of the sensor on the ear or fingertip can result in problems when used for RPSM. One problem is low blood perfusion, which can result in measurement errors [20], [30]. When peripheral circulation is impaired, arterial pulsations in the limbs are diminished [31], making it difficult to obtain accurate measurements. One situation where low perfusion could occur is during low temperatures [32]. Clearly, soldiers, hikers, or runners may encounter low ambient temperatures, making placement of the sensor on the fingertip or ear unsuitable for RPSM.

Specifically for finger placement, the degree of motion artifacts, which results in measurement error, has shown to be greater than other measurement sites for certain activities [33]. More importantly, however, a fingertip sensor can impede daily activities such as operating machinery and weapons.

2.5. Reflectance Mode Pulse Oximetry and Remote Physiological Monitoring

The use of reflectance mode pulse oximetry eliminates the sensor placement problems associated with transmission mode pulse oximetry because sensors can be placed on numerous body locations such as the chest, cheek, or forehead [34]. The variety of measurement sites is a major benefit for use with RPSM.

Placement of the sensor on the forehead has shown greater sensitivity to SpO_2 changes during low perfusion situations compared to other peripheral body locations [35], [36]. This attribute makes the forehead more effective for use during cold temperatures. The forehead has also shown to detect hypoxemia 90 seconds before a fingertip or ear sensor during peripheral vasoconstriction [37]. Also, a thin skin layer

coupled with a prominent bone structure helps to direct light back to the PD, providing strong PPG [38]. This allows for decreased LED drive current, thereby minimizing power consumption to lengthen battery life. Lastly, placement on the forehead has shown to result in decreased motion artifact during certain types of physical activity [33]. Due to the established benefits of forehead reflectance pulse oximetry, the remainder of the background is focused on this sensor type.

2.6. Limitations of Reflectance Pulse Oximetry for Remote Physiological Monitoring

There are two significant problems that must be overcome before reflectance pulse oximetry can be used effectively for RPSM. One problem is measurement error due to motion artifacts [39]. Any form of physical activity may lead to motion artifacts which corrupt the PPG signal and make accurate measurement of physiological parameters difficult if not impossible. The second problem is that the PPG signal is affected by pressure disturbances acting on the pulse oximeter probe, which can lead to the inability to measure SpO_2 and HR [8], [40] - [44].

2.7. Motion Artifacts

In relation to pulse oximetry obtained from the forehead, it is speculated that the main source of motion artifact is due to changes in the relative position of the sensor with respect to the frontal bone of the skull rather than the relative movements of the sensor with respect to the skin, as illustrated in Fig. 2.7. Due to the rounded and optically inhomogeneous surface properties of the skeletal bone, alterations in sensor position and orientation will cause changes in the distribution of R and IR backscattered light reaching the PD. Therefore, sudden changes in incident light intensity reaching the PD due to cyclical movement of the sensor will result in corruption of the PPG signal.

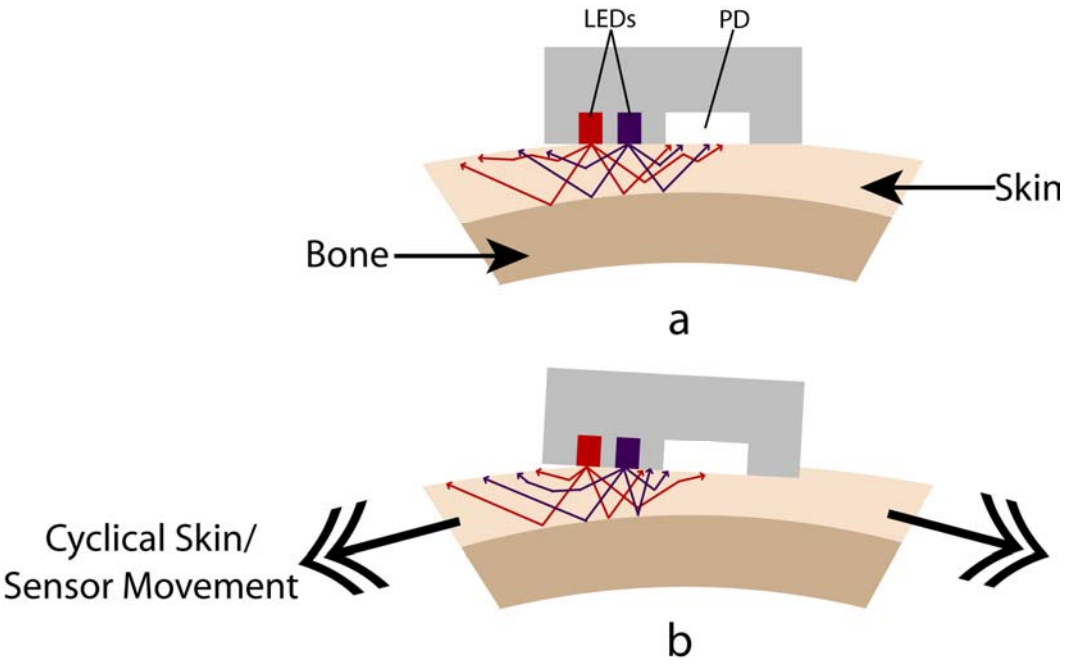

Figure 2.7. Sensor displacement as a major source of motion artifacts [21]. (a) typical light scattering before motion occurs, (b) motion induced cyclical movement causing changes in relative sensor position, changing the R and IR backscattered light reaching the PD.

Some research has also suggested that there may be two other sources of motion artifacts. The first source of motion artifacts can be attributed to the formation of air gaps created between the skin and sensor during physical activity [10], which may cause measurement error. Another source of motion artifact can be attributed to low venous pressure blood "slosh" with back and forth movement which is seen when an individual is physically active. This local perturbation of venous blood adds to the AC component of the PPG signal and can result in low oxygen saturation measurements [45].

Any source of motion artifact can result in a distorted PPG signal, as illustrated in Fig. 2.8, which would result in measurement inaccuracies. The figure shows that at the start of motion the PPG signal becomes corrupt with motion artifacts and is no longer identifiable.

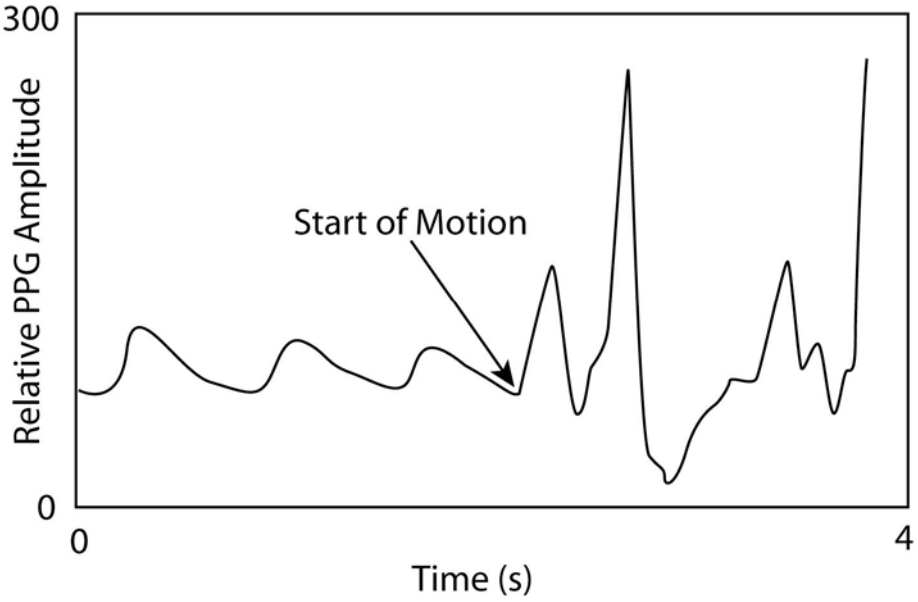

Figure 2.8. Effects of motion artifact on the PPG signal.

2.7.1. Minimizing Motion Artifact

Since the development of pulse oximeters, there have been numerous studies conducted in an attempt to overcome the effects of movement artifacts. These studies have investigated a variety of methods that improved measurement accuracy. However, measurement inaccuracy due to motion artifacts is still prevalent and limits the use of pulse oximetry for RPSM.

It is important to note that motion artifacts due to rigorous physical activity, such as running, will most likely not be eliminated completely. However, it can be assumed that if a subject is involved in rigorous activity, they are healthy. The most important situations where motion artifacts must be reduced are during times of moderate levels of activity, such as walking, because individuals can have health problems and still be able to walk. The following paragraphs discuss some previous methods and ideas aimed at artifact reduction and why improved methods of artifact reduction must be investigated.

2.7.2. Signal Processing

One common method to improve physiological measurements during motion is through signal processing, as reviewed by Hayes et al [46]. There have been numerous algorithms developed, with varying effects on measurement accuracy [47] - [50]. Of the most notable, Masimo (Irvin, CA), a leading pulse oximeter manufacturer, has developed advanced digital signal processing algorithms that have shown to significantly improve measurement accuracy [51] - [52]. Despite these improvements, measurement accuracy does not meet clinical standards [53].

Although signal processing has shown to improve measurement accuracy during motion, sophisticated algorithms require more powerful microprocessors which result in increased weight, size, and power consumption of the pulse oximeter. For remote monitoring applications where an individual must wear the unit over extended periods of time, the pulse oximeter must be small and lightweight, thus limiting the amount of signal processing that can be used. The sensor designed by our lab uses simple algorithms to minimize the size and weight of the device, therefore methods other than signal processing must be investigated.

2.7.3. Measurement Site

Past studies investigated whether a particular measurement site improves measurement accuracy. Dassel [54] and Mendelson [55] have shown that a reflectance mode sensor located on the forehead provides more consistent SpO_2 readings while a subject remains motionless and may provide more consistent readings in the presence of moderate amounts of motion artifacts as compared to other facial regions. Although these studies make the placement of the sensor on the forehead attractive, one must still be aware underlying issues with this measurement site. Mannheimer [56] has demonstrated that

placement of the sensor directly over larger cardio-synchronously pulsating or moving vasculature can result in SpO_2 inaccuracies. In this study, it was observed that placement of the sensor directly over the eyebrow slightly lateral to the iris avoids these inaccuracies.

Although selection of an appropriate measurement site can improve measurement accuracy, motion artifacts will be present no matter where the sensor is located. Therefore, other methods must be investigated to further reduce the effect of motion artifacts on pulse oximetry.

2.7.4. Signal to Noise Ratio

Some research suggests that the negative effects of motion artifacts on measurement accuracy can be improved if the signal to noise ratio (SNR) of the PPG signal is improved [49]. SNR is defined as:

$$SNR = \frac{P_{signal}}{P_{noise}} = \left(\frac{A_{signal}}{A_{noise}} \right)^2 \tag{3}$$

where, P is the power and A is the amplitude. For this discussion, the signal portion corresponds to the PPG and the noise portion corresponds to motion artifacts. SNR can be improved by increasing the P or A of the signal and/or decreasing the P or A of the noise. Since noise can only be reduced by reducing physical activity, designers rely on increasing the power of the PPG. However, motion artifacts are still present and therefore other reduction methods must be investigated.

2.7.5. Sensor Attachment

Current attachment methods, like that for the Nonin (Plymouth, MN) 8000R™ reflectance mode sensor, secure the sensor by means of a medical adhesive or headband [57]. The different types of reflectance sensors and attachment methods used in a clinical setting are shown in Fig. 2.9. Disposable probes typically use an adhesive tape for attachment. They are used for both short term and long term clinical monitoring, but must be discarded after approximately 12 hrs of use. Reusable sensors are normally attached using an adhesive tape or headband for longer term monitoring. Other attachment methods could be used provided that they are comfortable and user acceptable, such as integrating the sensor into pre-existing equipment like a soldier's helmet or goggles. Prior research suggests that a compressive headband is an optimal choice because it may prevent low pressure venous pulsations and venous pooling occurring especially when a subject is in the Trendelenberg position, which results in decreased SpO_2 readings [58]. However, other attachment methods capable of applying enough pressure to reduce the low pressure venous pulsations can be used.

Each of the attachment methods possess unique properties that may affect the degree of motion artifacts. Due to the effect of perspiration on adhesive tape, the possibly of the sensor losing contact with the skin is increased, resulting in increased motion artifacts or loss of contact with the skin. With a headband, there exists the possibility of the headband and sensor slipping off of the forehead, resulting in the inability to measure physiological data. To date, no studies have investigated whether the degree of motion artifacts, and therefore measurement accuracy, are different among the three attachment methods.

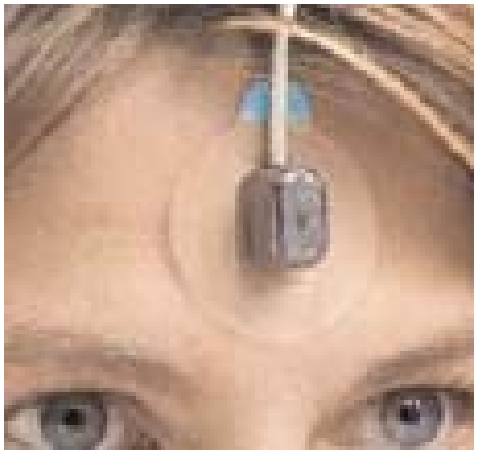

(a)

(b)

Figure 2.9. Different types of clinical attachment methods. (a). adhesive tape used with Nonin 8000R™ [57], (b). headband used by Nellcor reflectance sensors [59].

2.7.6. Contact Pressure

Several studies were conducted to aid in understanding how contact pressure affects pulse oximetry measurements. These studies provide a qualitative description of the effect of contact pressures on the PPG signal and its components [10], [40] - [42]. When the contact pressure used to secure the sensor to the body is too low, distorted PPG waveforms can occur, resulting in inaccurate measurements [60]. If the contact pressure is too high, blood circulation can be compromised or necrosis could occur if the sensor is worn for extended periods of physical activity [61]. With compromised blood circulation, the ability to measure SpO_2 is also reduced [62]. Also, with large contact

pressures, complete vessel occlusion can occur, leading to a complete loss of the PPG signal and the ability to obtain SpO_2 and HR measurements [61].

Teng [42] observed that the AC amplitude of the PPG signal from a fingertip sensor increases and then decreases with increasing contact pressure. The effect of contact pressures on the AC amplitude of the PPG signal as observed by Teng is shown in Fig. 2.10.

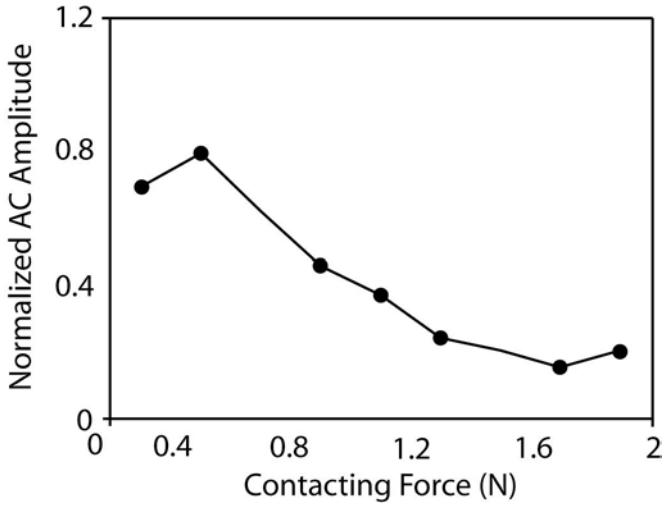

Figure 2.10. Effects of contacting force on AC amplitude redrawn from Teng [42].

The optimal contact pressure will result in the greatest AC amplitudes because during physical activity, when motion artifacts introduce added signal noise, SNR will be the highest, which may result in improved measurement accuracy. Therefore, Teng's study suggests that a contacting force of approximately 0.32 N is optimal. However, due to physiological differences, the same results may not be observed from a reflectance sensor located at the forehead.

Dassel [40], [41] observed the effects of contact pressure on the PPG amplitude of a forehead reflectance sensor. The studies showed that amplitudes initially increased but subsequently decreased when the subject pushed on the sensor. However, the effects of

pressures between those that caused an increase in amplitude and the pressure exerted when pushing on the sensor were not investigated. Therefore, the pressure causing the decrease in amplitude was not determined and an optimal contact pressure or range of pressures for a forehead reflectance sensor cannot be determined from previous studies. Also, no studies investigated if optimal contact pressures, resulting in large PPG amplitudes, lead to measurement improvement during motion artifacts.

2.8. Pressure Disturbances

Even if an attachment method providing an optimal contact pressure is utilized to secure a reflectance sensor to the forehead, there is no current technology that can prevent other pressure disturbances, such as a soldier being injured and falling on the sensor. In this situation, pressures may be great enough to cause a complete loss of the PPG signal and the ability to measure SpO_2 and HR during this critical time.

To reduce these effects, Rhee designed the finger-ring pulse oximeter shown in Fig. 2.11 [63]. It can be worn on a subject's finger like a ring and consists of an internal and external band. The internal band contains the sensor. When external pressures are applied to the ring, the external band moves but the internal band remains in contact with the finger at a constant pressure, as illustrated in Fig. 2.12. However, this device would not work for a reflectance forehead sensor. In addition, if the external force is applied perpendicular to the optical components, which would occur if this device was placed on the forehead and a subject fell on it, the vasculature underneath the outer ring would become occluded, thus blood supply to the optical components would be compromised.

Figure 2.11. Transmission mode finger-ring sensor for reduction of pressure effects [63].

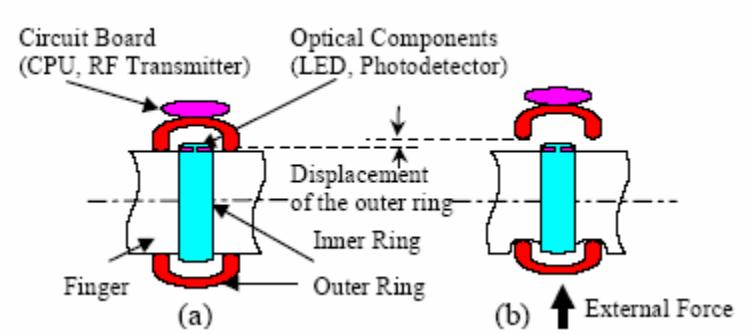

Figure 2.12. Transmission mode finger-ring sensor designed by Rhee et al [64].

3. RESEARCH OBJECTIVES

Although steady progress has been made in the development of a more robust wearable forehead pulse oximeter, current technology has yet to be proven effective for RPSM. Two significant limitations of current technology include measurement errors attributed to motion artifacts and pressure disturbances. Furthermore, little attention has focused on the method of sensor attachment for motion artifact reduction or sensor housings designs that could reduce the effects of pressure disturbances on a wearable forehead reflectance pulse oximeter. Therefore,

The main research objective was to determine if sensor housing and mounting options can improve the accuracy of measurements from a wearable forehead pulse oximeter.

The specific aims of this thesis were as follows:

Specific Aim 1 - To determine the effects of mounting options on the accuracy of SpO_2 and HR from a wearable forehead pulse oximeter sensor during walking.

Specific Aim 2 - To determine the effects of housing options on the accuracy of SpO_2 and HR from a wearable forehead pulse oximeter sensor in the presence of pressure artifacts.

4. METHODS

The following sections discuss the methodology used for achieving the main research objective and its specific aims.

4.1. Specific Aim 1 - Effects of Mounting Options

Several studies were conducted to determine the effects of mounting options on the accuracy of SpO_2 and HR from a wearable forehead pulse oximeter sensor. The primary goal of these studies was to determine a mounting option that minimizes motion artifacts, thereby improving SpO_2 and HR accuracy during motion. The studies consisted of:

- Determining an optimal contact pressure range for sensor attachment.
- Determining if optimal contact pressures result in improved SpO_2 and HR when motion artifacts are present.
- Determining if a particular sensor attachment method can improve measurement accuracy during walking.

4.1.1. Optimal Contact Pressure(s)

Ten volunteers, 21 - 24 years old, took part in this study to determine an optimal contact pressure range for sensor attachment to the forehead. Based on preliminary measurements, shown in Appendix A, n = 10 allows for the identification of an optimal contact pressure range with a 0.05 confidence level and margin of error less than 15%.

Fig. 4.1 illustrates the experimental setup. Two commercial Nonin™ (Plymouth, MN) reflectance sensors acquired analog PPG signals. The sensors were chosen for two reasons. First is the data is of the ASCII format, which makes data recording easy. The second reason is that there is minimal signal processing, as compared to other current sensors, thereby allowing the full effects of motion artifacts to be observed. Separate

Nonin Xpods extracted SpO_2 and HR data from the signal. A National Instruments 4 port RS-232 serial-to-USB hub allowed for the simultaneous measurement of the digital PPG, SpO_2, and HR data. The output of the hub was connected to a laptop PC outfitted with a custom LabVIEW software program for simultaneously recording of data in real-time. Refer to Appendix B for the LabVIEW diagram. A compressive load cell (MSI, Hampton, VA) was used to measure the force applied on the forehead sensor. The LabVIEW program subsequently converted the force to pressure, assuming that

$$P = \frac{F}{A} \tag{4}$$

where, P is the pressure, F is the force, and A is the area of the sensor in contact with the skin.

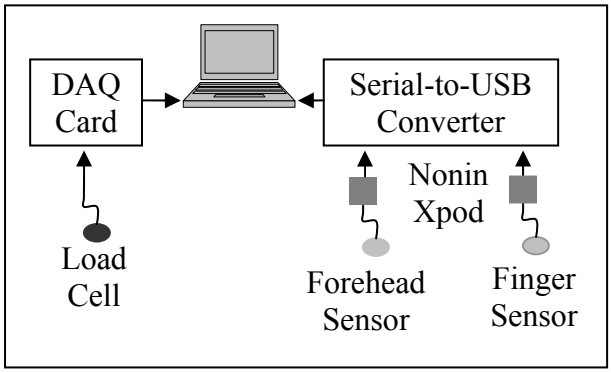

Figure 4.1. Experimental setup for real-time pressure, PPG, SpO_2, and HR measurement from Nonin reflectance sensors.

The subject rested in a comfortable prone position. One pulse oximeter sensor was centered above the eyebrow. A second sensor was attached to the subject's fingertip and served as an independent measurement site. The individual was instructed to rest the hand that the fingertip sensor was attached to on a table. With the other hand, they were instructed to exert a pressure on the middle of the sensor, according to the pressure displayed on the PC. Pressures were changed from 30 - 300 mmHg in approximately 25

mmHg step increments. Data were collected for 20 s intervals at each pressure level at a rate of 75 samples per second.

Post data acquisition, the data files were loaded into a custom MATLAB software program (Appendix C) that detected the positive and negative peaks of the PPG associated with one cardiac cycle. The difference in peak amplitudes results in the peak-to-peak amplitude of the PPG for that heart cycle. For a given pressure level, the program calculated the mean peak-to-peak amplitude of the PPG and the SpO_2 and HR errors, where the error was defined as the (forehead - fingertip) data.

A second study was undertaken to study the effects of attaching a pulse oximeter sensor with an optimal contact pressure on SpO_2 and HR error during walking. Initially ten volunteers, 19 - 24 years old, took part in this study. Based on the measured data, n = 10 allows for a one-way ANOVA calculation for differences in measurement error with a power of 0.9 and a confidence level of 0.05, which is greater than the standard confidence level of 0.05 with a power of 0.8. Therefore, additional volunteers were not needed.

The experimental setup illustrated in Fig. 4.1 was used to collect the data for this study, with the exception of a new LabVIEW program (Appendix D). The forehead sensor was fitted inside a custom housing, shown in Fig. 4.2, and secured to the forehead with an elastic band. The housing was fabricated to accommodate the Nonin™ reflectance sensor, and was manufactured from black Delrin® to absorb ambient light. Refer to Appendix G for the schematic. Three independent trials were conducted. In each trial, the sensor was secured at a different contact pressure. The contact pressure was measured by the load cell before the onset of walking. The contact pressures investigated were chosen based on the results of the above study, shown in Fig. 5.1, such that the

effects of low (30 mmHg), optimal (80 mmHg), and high (200 mmHg) contact pressures could be studied.

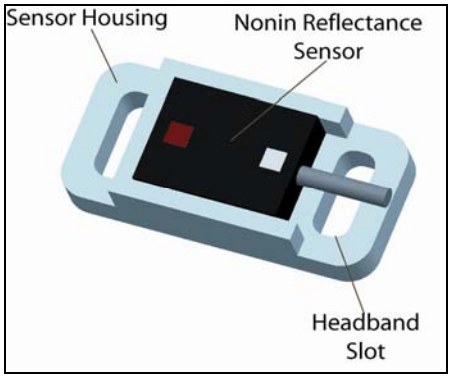

Figure 4.2. Custom sensor housing for attachment to the forehead with an elastic band.

Walking can create rhythmic motion artifacts associated with each step. If motion artifacts completely corrupt the PPG signal, there is a possibly that the artifacts could resemble a PPG signal and HR data could reflect the frequency of oscillations due to stepping. A pace of 4 mph translates to approximately 350 steps/min. Therefore, if the pulse oximeter misinterprets the motion as the PPG signal, HR data could read as high as 350 bpm, which clearly indicates measurement error. If a lower walking pace were chosen, the frequency of steps could be within possible HR ranges, making it difficult to determine if HR data represented that from the PPG or from the rhythmic motion artifacts.

Subjects were instructed to rest their hand with the fingertip mounted sensor on the treadmill's support rail so that reference PPG signals free of motion artifacts could be obtained. The treadmill's speed was set to a moderate-walking pace of 4 mph and the subjects were instructed to maintain this pace for 2 min. during data acquisition.

After data were acquired, the reference signal was inspected and if significant instances of motion artifacts were detected, they were deleted from both data sets.

Significant motion artifacts were defined as SpO_2 and HR changes greater than 5 % or bpm, respectively, in one second as they are not realistic changes. SpO_2 values greater than 100% and less than 95% were indications of motion artifacts as these values are not likely for a healthy individual. Furthermore, HR values les than 50 bpm or greater than 175 bpm were also treated as motion artifact related errors. As a further method of signal inspection, data where the PPG signal was completely lost was deleted.

Post signal inspection, a dedicated MATLAB program (Appendix E) calculated the mean absolute SpO_2 and HR errors. The program also detected SpO_2 and HR measurement dropouts and recorded the percentage of dropouts. Dropouts were defined as SpO_2 measurements equal to 0% or greater than 100 % and HR measurements equal to 0 bpm or 255 bpm.

4.1.2. Sensor Attachment Methods

Three separate 10 hour long hikes were undertaken as a preliminary field study to investigate the feasibility of securing a sensor to the forehead over extended periods of physical activity for various attachment methods. The attachment methods studied consisted of an FDA approved adhesive tape (Part # 1577, 3M, St. Paul, MN), shown in Fig. 4.3 and 4.4, an elastic headband (Fig. 4.5 and 4.6), and sewing the sensor to the headband of a military helmet (Fig. 4.7 and 4.8).

The elastic band and adhesive tape were chosen as they can be used in a variety of situations, such as runners, hikers, and soldiers. A headband is frequently worn for activities such as running so it is comfortable to wear and users would not have to wear an added piece of equipment to secure the sensor. The adhesive tape was chosen as an alternative for users who may not want to wear a headband. The tape is clear so that it

does not draw added attention to it, which is important for civilian use. On the other hand, both the headband and adhesive can be easily camouflaged for military use. The adhesive tape chosen was selected over other types because it was FDA approved for long term use and was proven to stay in contact with the skin for 21 days with minimal skin irritation. As the military is the main consumer target group for wearable pulse oximetry, integration of the sensor into pre-existing equipment is required. Besides a helmet, goggles are the only other piece of equipment that is secured to the forehead region. However, a helmet is worn more frequently than goggles, and therefore the appropriate choice.

The 3M medical adhesive field study consisted of a 10.25 hr hike that spanned 10.62 miles over varying forest terrain. Temperatures were in the upper 80's °F with high humidity (>80%). The field study for the elastic headband and the integration of the sensor inside of a military helmet consisted of a 10 hr hike that spanned 9.35 miles over varying forest terrain. Temperatures were in the mid 70's °F with high humidity. The hikes were chosen during these environmental conditions so that perspiration would be prevalent.

At varying time and distance intervals, the subject was instructed to remain still and SpO_2 and HR were recorded from the Nonin^{TM} reflectance sensor positioned in the middle of the forehead. A second sensor attached to the fingertip only while the subject remained still, served as a reference.

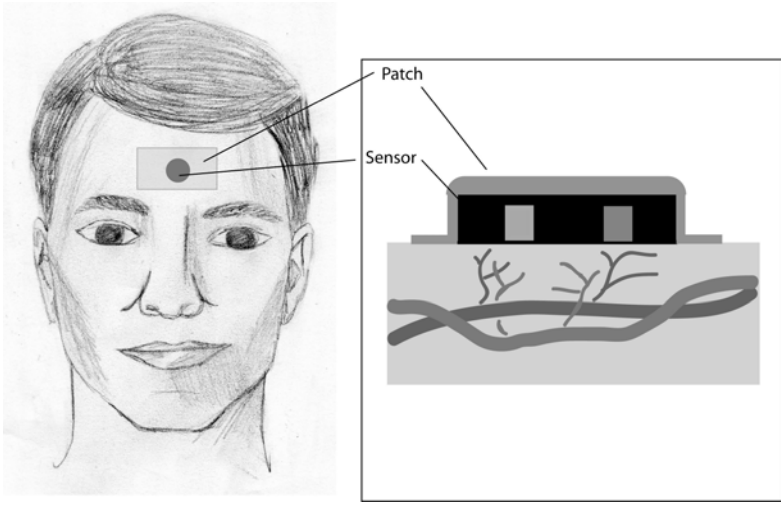

Figure 4.3. Illustrated view of medical adhesive method for sensor attachment to the forehead [21].

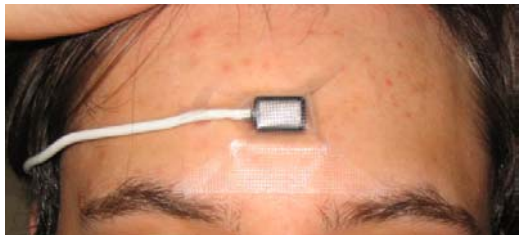

Figure 4.4. Medical adhesive placed over the sensor for attachment to the forehead.

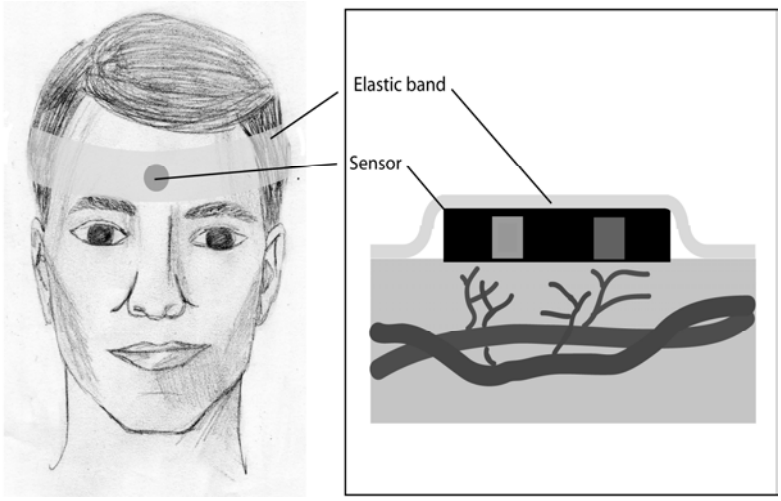

Figure 4.5. Illustrated view of elastic headband attachment to the forehead [21].

Figure 4.6. Elastic headband used for sensor attachment to the forehead.

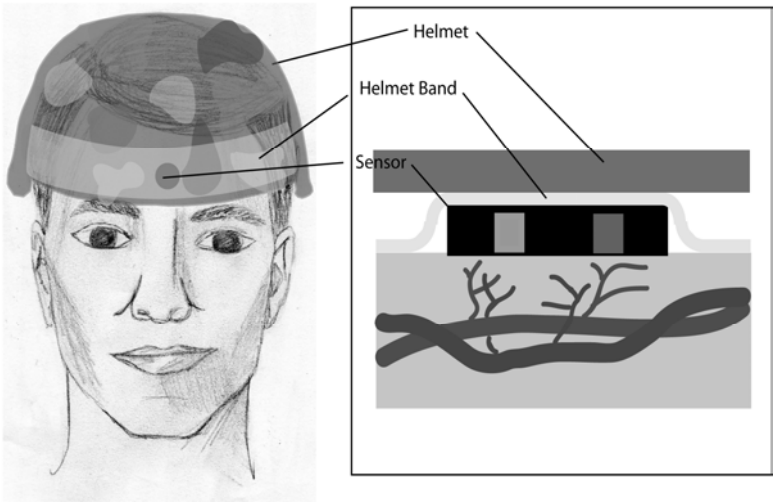

Figure 4.7. Illustrated view of helmet method for sensor attachment to the forehead [21].

Figure 4.8. Securing the sensor to the inner lining of a helmet for attachment to the forehead.

Fig. 4.9 illustrates the experimental setup. The two pulse oximeters were connected to a National Instruments RS-232 4 port serial-to-USB hub connected to a laptop PC. A custom LabVIEW software program (Appendix D) acquired HR, SpO_2, and the PPG data simultaneously, in real-time, from each sensor. After the hikes, a dedicated MATLAB program (Appendix E) was utilized to calculate HR and SpO_2 error for each 2 min. interval of data.

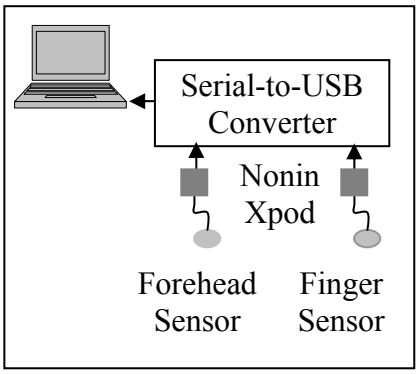

Figure 4.9. Experimental setup for real-time PPG, SpO_2, and HR measurement from Nonin reflectance sensors.

A second study was conducted during walking by recording SpO_2 and HR data from the forehead of ten volunteers, 19 - 24 years old, using the three different sensor attachment methods described in Fig. 4.3 - 4.8. Based on the measured data from this study, an n = 10 allows for comparison of data with a one-way ANOVA having a confidence level of 0.05 and a power of 0.98, which is greater than the standard confidence level of 0.05 with a power of 0.8. Therefore, additional volunteers were not needed. The same experimental setup as described in section 4.1.1 was utilized.

4.2. Specific Aim 2 - Effects of Housing Options

A study was conducted to investigate the effects of housing options on the accuracy of SpO_2 and HR measurements from a wearable forehead pulse oximeter. Refer to Appendix D for a discussion of the housing options investigated.

Ten volunteers, 19 - 24 years old, took part in this study. Both designed housings, as described in Appendix G, and a control housing, shown in Fig G.1, were studied. The ability for each of the three housings to maintain blood supply to the sensor in the presence of pressure disturbances were separately studied, such that 3 independent measurement sets were obtained for each individual. Based on the measured PPG data from this study, n = 10 provides the ability to detect PPG amplitude differences between the control and designed housings of 0.1 with a confidence level of 0.05 and a power of 0.9, which is greater than the standard confidence level of 0.05 with a power of 0.8. Therefore, additional volunteers were not needed.

The experimental setup shown in Fig. 4.1 and described in Section 4.1.1 was utilized. The exception is that the pressure range investigated ranged from 200 - 1200 mmHg so that pressures possibly occurring should an individual fall on the sensor could be studied. The possible pressures were determined by measuring the pressure exerted by the subject's head on a table. A 95% confidence interval was then constructed, yielding a pressure range from 600 - 1200 mmHg.

5. RESULTS

5.1. Specific Aim 1 - Effects of Mounting Options

5.1.1. Optimal Contact Pressure Range

Fig. 5.1 illustrates the effects of contact pressure on PPG amplitudes which were normalized to the largest observed amplitude for each individual. Each point on the graph represents the mean normalized amplitude for all 10 individuals. The 95% confidence intervals were calculated for each point to determine if the observed amplitude was statistically within an optimal range, which was defined as pressures yielding normalized amplitudes greater than 0.7. A value of 0.7 was chosen as the nominal threshold because preliminary data suggested that this would be the maximal value that could be statistically identified without relying on extremely large samples greater than 150. The yellow regions indicate contact pressures that do not provide optimal amplitudes. The blue regions represent instances where the confidence interval produced amplitude values greater or less than 0.7, therefore, optimal amplitude in these regions is questionable. The region from 60 - 80 mmHg represents optimal contact pressures. Please refer to Appendix F for a detailed discussion regarding why and how the data was normalized and the graph constructed.

Fig. 5.2 illustrates the effects of contact pressure on SpO_2 and HR errors while the subject remained motionless for the designated contact pressure ranges shown in Fig. 5.1. Because the mean error for the population was not normally distributed, Kruskal-Wallis one-way ANOVA on ranks was conducted. The test indicated that measurement errors are not affected by the contact pressures studied ($p = 0.77$). Additionally, mean

measurement errors do not exceed the specified accuracy of the device (± 2 digits for SpO_2 and HR).

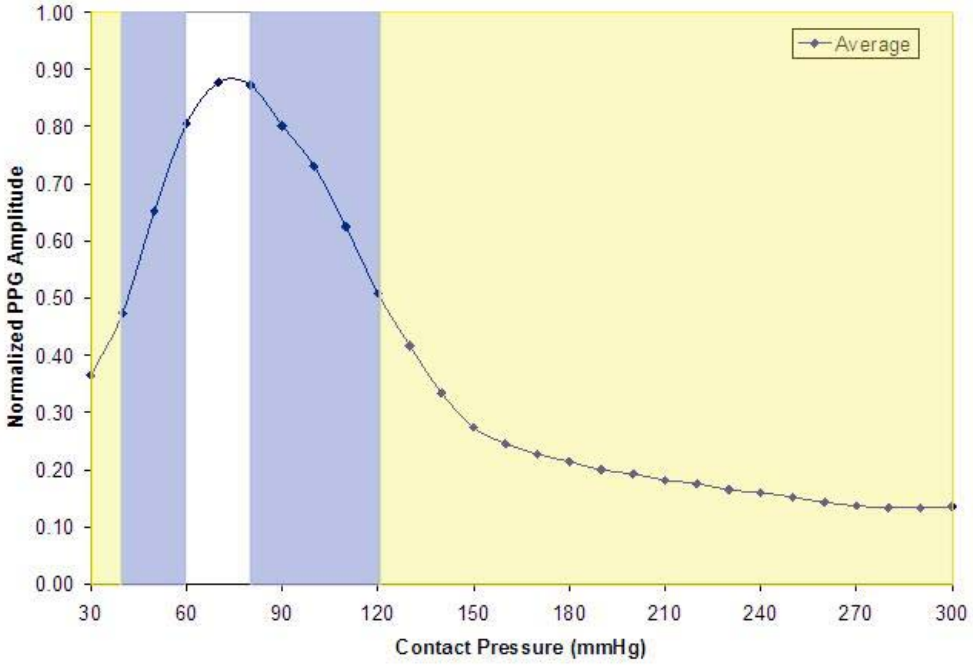

Figure 5.1. Effects of contact pressure on normalized PPG amplitude (yellow - not optimal, blue - indeterminate, white - optimal).

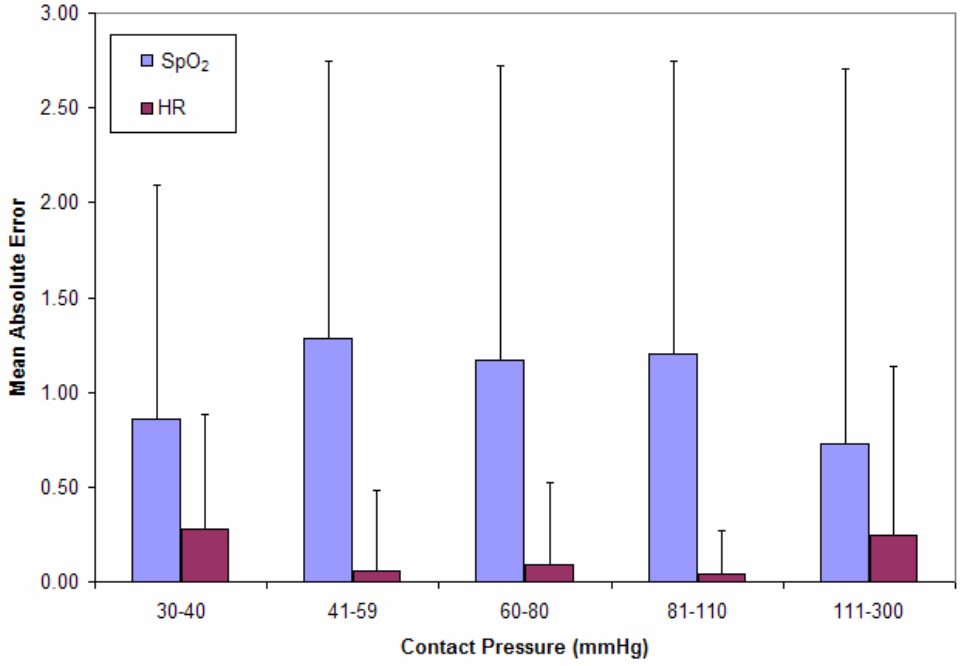

Figure 5.2. Effects of contact pressure on mean absolute SpO_2 (%) and HR (bpm) errors during rest (Vertical line represents +1 SD).

Fig. 5.3 shows the effects of contact pressures on measurement dropouts, and SpO_2 and HR errors from 3 different pressure regions defined in Fig. 5.1, where 30 mmHg was considered low and not optimal, 80 mmHg as optimal, and 200 mmHg as high and not optimal. As the data were not normally distributed, Kruskal-Wallis one-way ANOVA on ranks was conducted. The test concluded that there is a statistically significant difference in the percentage of measurement dropouts, and HR and SpO_2 measurement errors for the contact pressure of 80 mmHg vs. 30 mmHg, indicating that measurement error is reduced when a contact pressure of 80 mmHg is utilized ($p<0.05$). The tests also concluded that there is a significant improvement in dropouts and SpO_2 error for a contact pressure of 200 mmHg vs. 30 mmHg. It was concluded that no statistically significant difference exists in the percentage of measurement dropouts, and HR or SpO_2 measurement errors for 80 mmHg vs. 200 mmHg. A summary of the results are shown in Table 1.

Table 1. Summary of Kruskal-Wallis tests for effects of contact pressures on measurement error during walking.

Comparison	Dropout Percentage Significant ($p<0.05$)?	SpO_2 Error Significant ($p<0.05$)?	HR Error Significant ($p<0.05$)?
80 mmHg vs. 30 mmHg	Yes	Yes	Yes
80 mmHg vs. 200 mmHg	No	No	No
30 mmHg vs. 200 mmHg	Yes	Yes	No

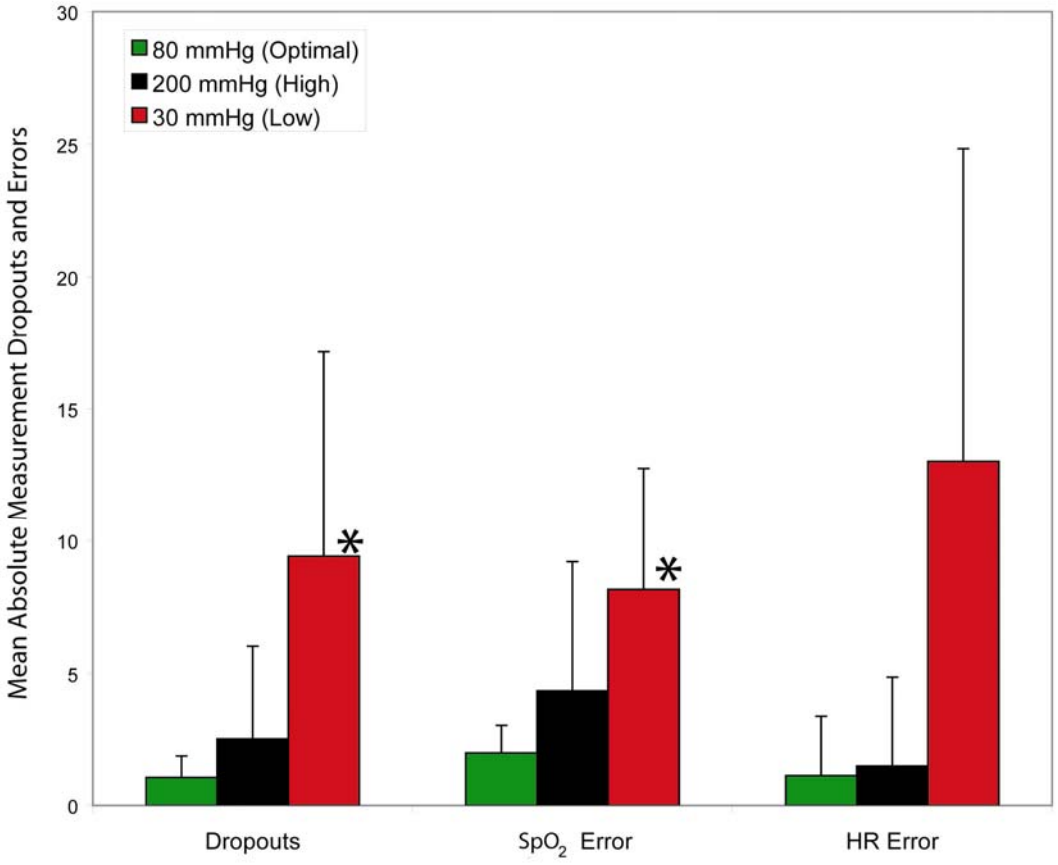

Figure 5.3. Effects of different contact pressures on percentage of measurement dropouts and SpO_2 (%) and HR (bpm) errors during walking. (Vertical line represents +1 SD; asterisk indicates a statistically significant difference in the group).

5.1.2. Sensor Attachment Methods

Fig. 5.4 - 5.6 show typical resting PPG signals obtained at the end of the 10 hr. hike from the forehead sensor that was secured by an adhesive tape, elastic band, and integration into a military helmet. Each attachment method shows identifiable PPG signals, indicating that the sensor could be properly secured over extended periods of physical activity.

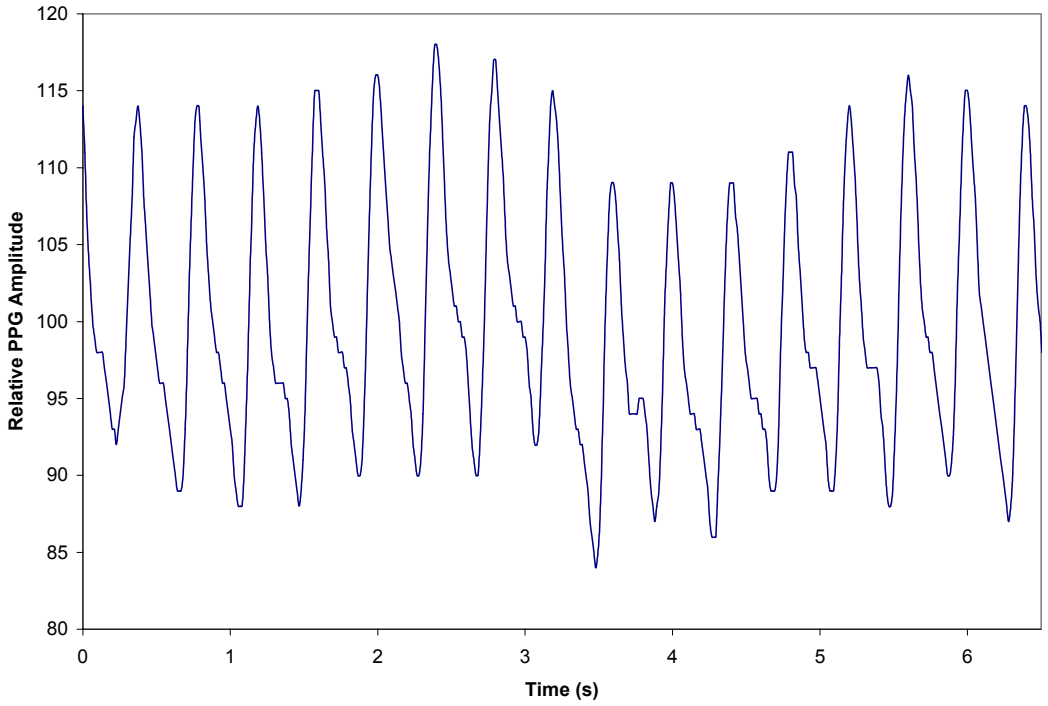

Figure 5.4. Typical resting PPG signal obtained from an adhesive tape mounted forehead sensor after extended periods of activity.

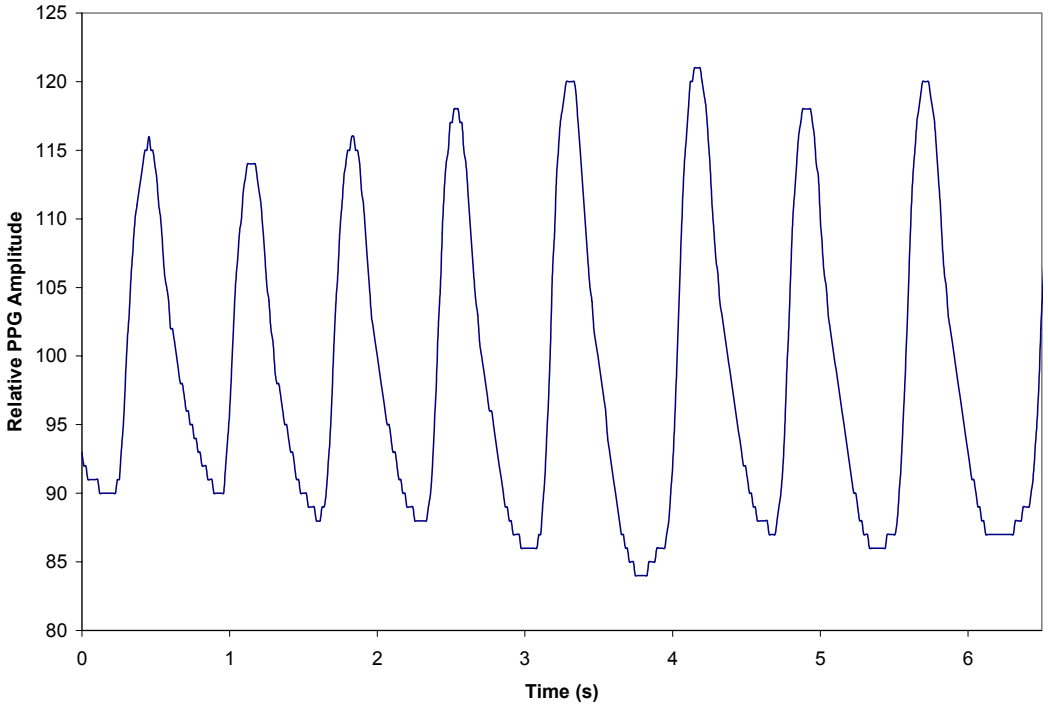

Figure 5.5. Typical resting PPG signal obtained from a headband mounted forehead sensor after extended periods of activity.

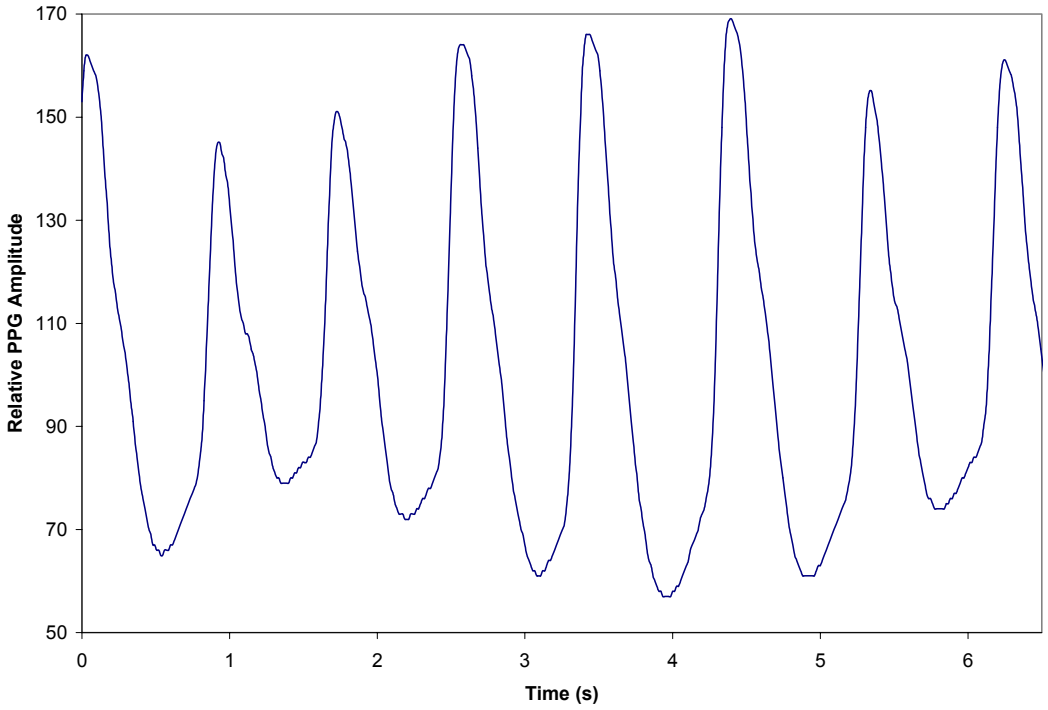

Figure 5.6. Typical resting PPG signal obtained from a helmet integrated forehead sensor after extended periods of activity.

Fig. 5.7 shows the mean absolute error for all resting SpO_2 and HR errors for sensor attachment by means of the three attachment methods during preliminary field studies. All errors are below the specified accuracy of the device (± 2 digits for SpO_2 and HR). One-way ANOVA statistical analysis concluded that there was no statistically significant measurement error between all 3 attachment methods, indicating that each attachment method keeps the sensor in proper contact with the skin over extended periods of physical activity ($p = 0.07$ for HR, $p = 0.46$ for SpO_2).

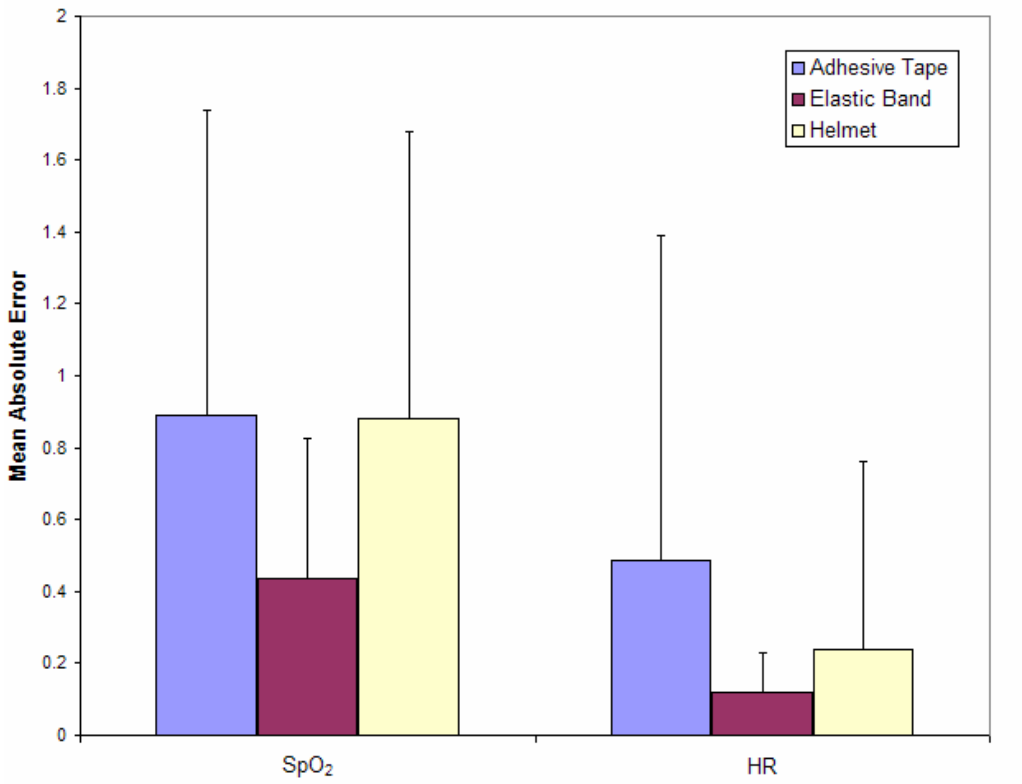

Figure 5.7. Resting mean absolute SpO_2 (%) and HR (bpm) errors for sensor attachment methods during field studies. Vertical line represents +1 SD.

Fig. 5.8 shows the effects of feasible sensor attachment methods on measurement dropouts, and SpO_2 and HR errors during walking. Kruskal-Wallis one-way ANOVA on ranks concluded that there is a statistically significant difference in the percentage of measurement dropouts, and HR and SpO_2 measurement errors for sensor attachment using an elastic band vs. integration of the sensor inside a military style helmet ($p<0.05$). The tests also concluded that there is a statistically significant difference in the percentage of measurement dropouts and HR measurement errors for sensor attachment using an elastic band vs. an adhesive tape. A summary of the results is shown in Table 2.

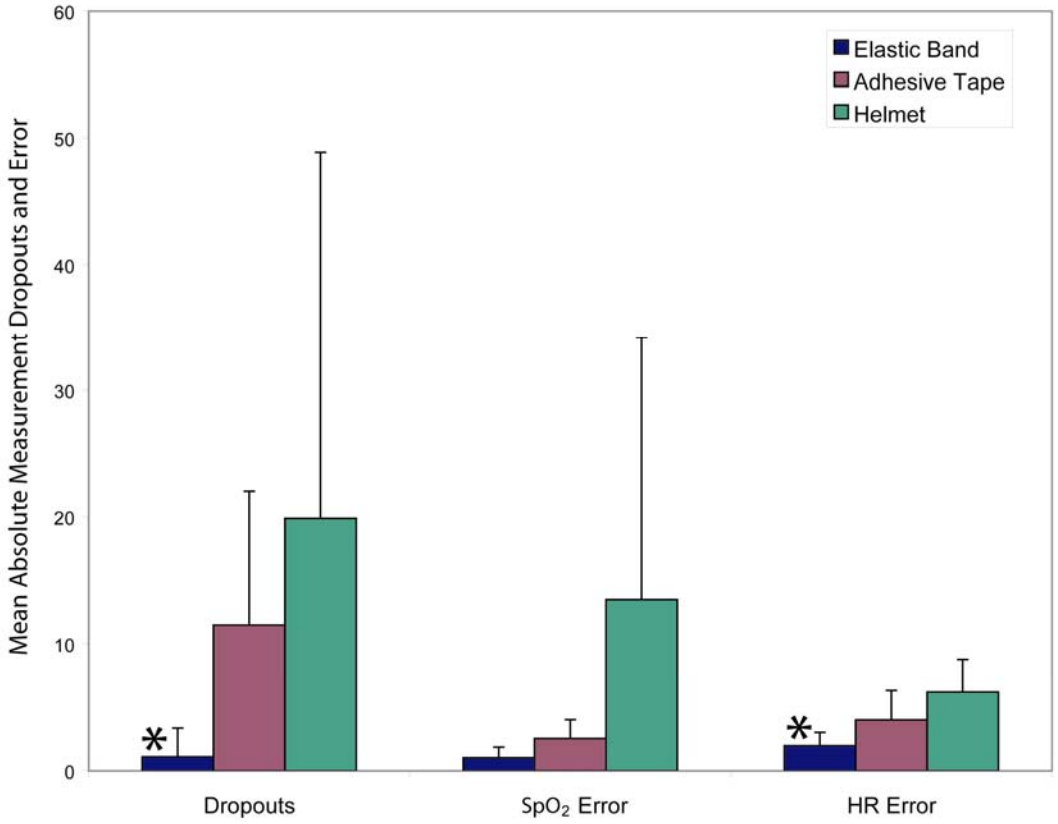

Figure 5.8. Effects of sensor attachment methods on SpO_2 and HR dropouts and errors during walking (Vertical line represents +1 SD; asterisk represents statistically significant difference in groups)

Table 2. Summary of one-way ANOVA tests for effects of sensor attachment methods on SpO_2 and HR dropouts and errors during walking.

Comparison	Dropout Percentage Significant ($p<0.05$)?	SpO_2 Error Significant ($p<0.05$)?	HR Error Significant ($p<0.05$)?
Elastic Band vs. Helmet	Yes	Yes	Yes
Elastic Band vs. Adhesive Tape	Yes	No	Yes
Helmet vs. Adhesive Tape	No	No	No

5.2. Specific Aim 2 - Effects of Housing Options

Fig. 5.9 shows the effects of contact pressure on normalized PPG amplitude when the control and the two designed housings are implemented. The points on the graph represent the mean amplitude for the 10 trials, which are connected by a smooth line to help in visualizing the trend. The green shaded region illustrates pressures that exist occur should a person fall on the sensor. The plot was constructed in a similar manner as Fig. 5.1. Refer to Appendix F which provides the details of plot construction. A Kruskal-Wallis one way analysis of variance on ranks concluded that the differences in the median values of normalized amplitude among the treatment groups are greater than would be expected by chance, indicating that there is a statistically significant difference in amplitude when the designed housings are utilized ($p = 0.001$). Additionally, a Tukey test was conducted to compare the measured amplitudes for each housing. This test allows for a multiple comparison of mean ranks, rather than median ranks used for the Kruskal-Wallis tests, and is less likely to determine that a given difference is statistically significant. The test concluded that there is a statistically significant difference between both Housing 1 and 2 compared to the control housing, indicating that the designed housings provide larger amplitudes over the studied pressure range. The tests showed no statistically significant difference between Housing 1 and 2.

Fig. 5.10 shows the effects of contact pressure on SpO_2 measurement error for various pressure regions for each of the three housings investigated. Kruska-Wallis one-way ANOVA on ranks was conducted for each of the pressure regions shown in Fig. 5.10. The results of these tests are summarized in Table 3. The tests concluded that there is not a statistically significant difference between the two designed housings at any pressure level. For Housing 1 vs. the control and Housing 2 vs. the control, the tests

concluded that SpO_2 measurement error is improved for pressures greater than 301 mmHg ($p<0.05$).

Fig. 5.11 shows the effects of contact pressure on HR measurement error for various pressure regions for each of the three housings investigated. One-way ANOVA on ranks was conducted for each of the pressure regions shown in Fig. 5.11. The tests concluded that there is a statistically significant difference between the two designed housings and the control at pressure greater than 601 mmHg ($p>0.05$).

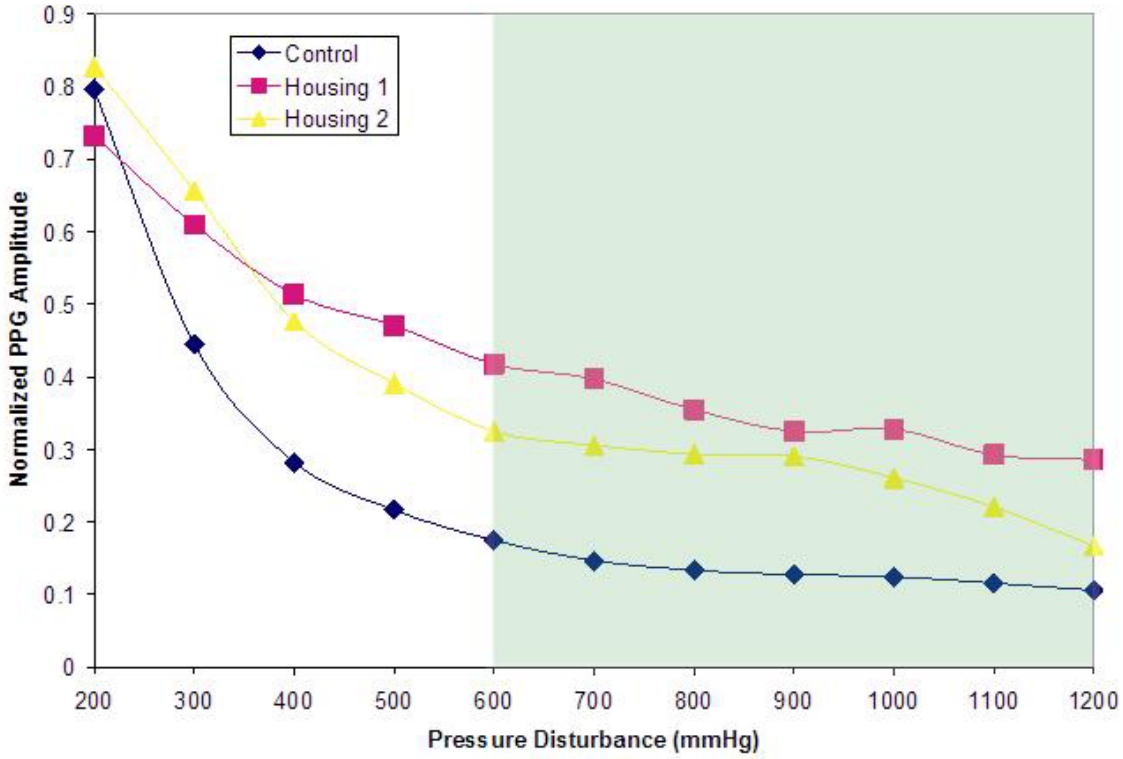

Figure 5.9. Effects of contact pressure on normalized PPG amplitude for the control and designed housings. Green shaded region indicates pressure that could be exerted should a person fall on the sensor.

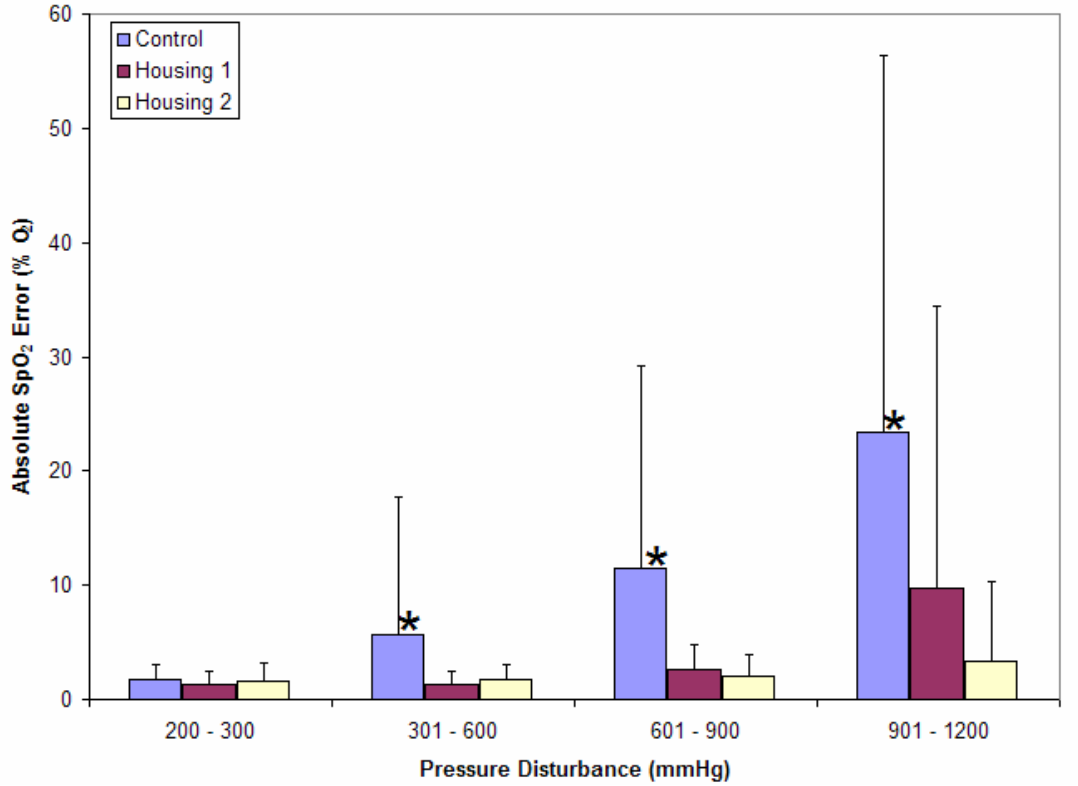

Figure 5.10. Effects of external pressure on mean absolute SpO_2 error for the control and designed housings. Asterisk represents statistically significant difference in group.

Table 3. Results of ANOVA comparison of SpO_2 error utilizing the different housings.

Pressure Range (mmHg)	p<0.05 (Control vs. Housing 1)	p<0.05 (Control vs. Housing 2)	P<0.05 (Housing 1 vs. Housing 2)
200 - 300	No	No	No
301 - 600	Yes	Yes	No
601 - 900	Yes	Yes	No
900 - 1200	Yes	Yes	No

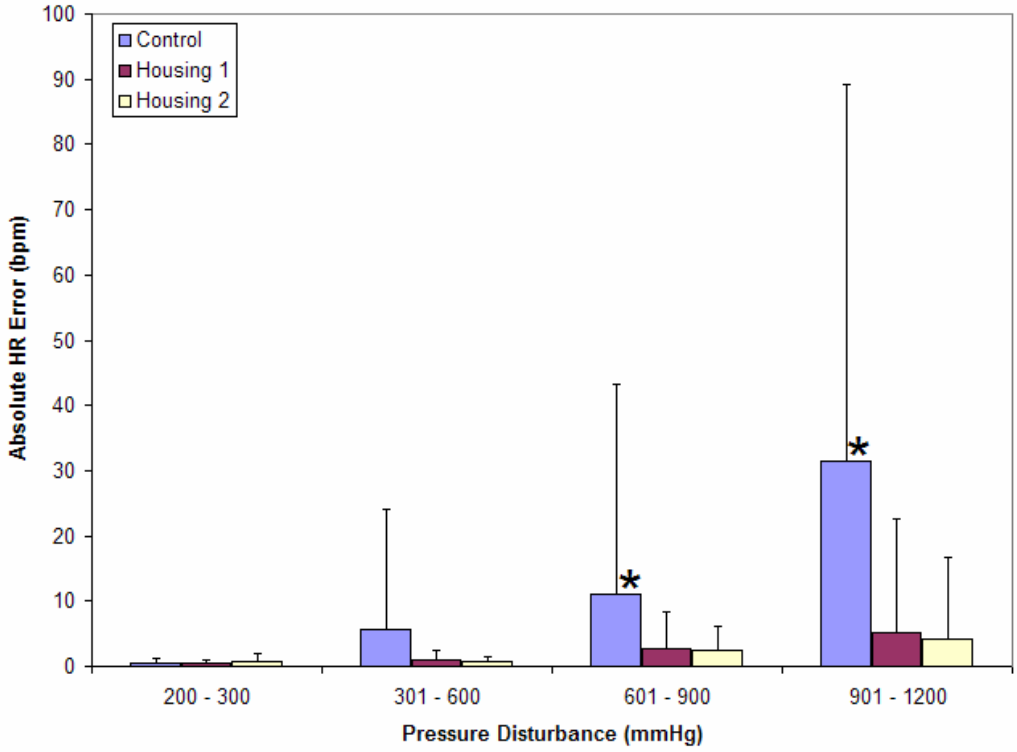

Figure 5.11. Effects of external pressure on mean absolute HR error for the control and designed housings. Asterisk represents statistically significant difference in group.

Table 4. Results of ANOVA comparison of HR error utilizing the different housings.

Pressure Range (mmHg)	p<0.05 (Control vs. Housing 1)	p<0.05 (Control vs. Housing 2)	p<0.05 (Housing 1 vs. Housing 2)
200 - 300	No	No	No
301 - 600	No	No	No
601 - 900	Yes	Yes	No
901 - 1200	Yes	Yes	No

6. DISCUSSION

6.1. Specific Aim 1 - Effects of Mounting Options

6.1.1. Optimal Contact Pressure

The observed effects of contact pressure on PPG amplitudes shown in Fig. 5.1 follow a similar trend observed by Teng [42]. These effects can be attributed to changes in reflected light intensity. When the initial pressure beyond that used to secure the sensor is applied, the tissue underneath starts to compress. This decreases the light absorption during diastole, shifting the diastolic peak down, as illustrated in Fig. 6.1. Since the arterial vasculature network is not significantly affected by these low pressures, the systolic peak remains at the same value. Therefore, the result is an initial increase in the PPG amplitude. However, once arterial constricting pressures are reached, the volume of pulsatile blood is decreased, resulting in a decrease in the PPG amplitude.

The data suggests that contact pressures ranging from 60 - 80 mmHg result in normalized amplitudes greater than 0.7. As mentioned previously, large samples greater than 150 would be required to identify a smaller more precise range of pressures producing normalized amplitudes greater than the chosen threshold of 0.7. The requirement for a large sample size is due to the variability of pressures causing the largest observed amplitude. This variability is most likely attributed to physiological differences between subjects and is the reason why the mean normalized amplitude does not reach a value of 1, which could only be achieved if every individual exhibited the greatest amplitude at the same contact pressure.

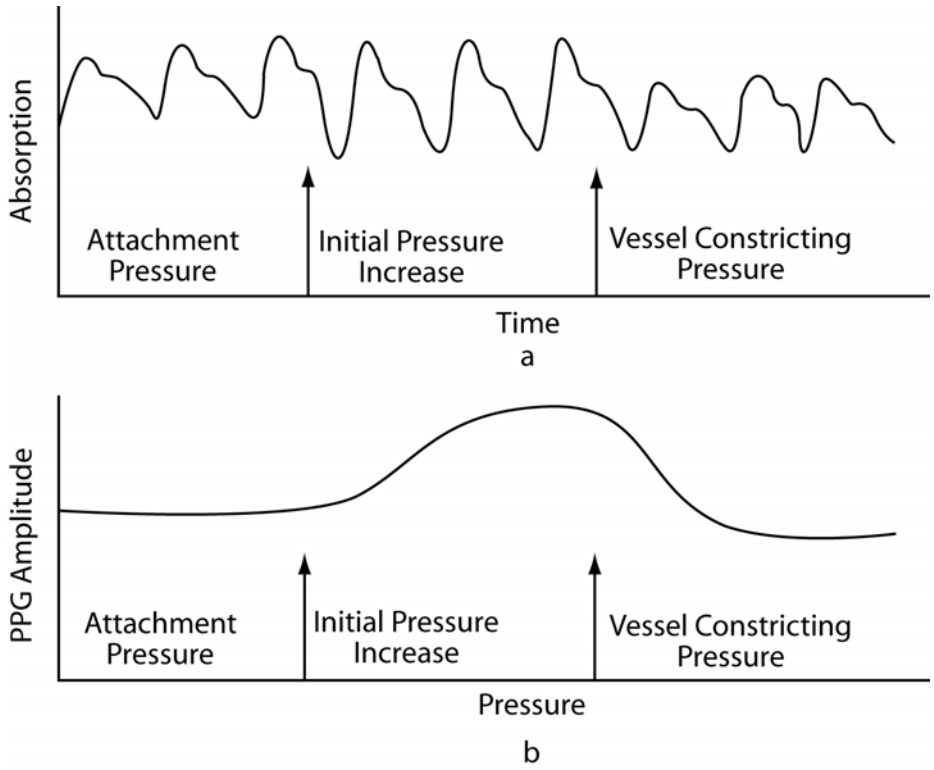

Figure 6.1. Illustrated changes in DC values result in PPG amplitude changes. (a). Initial increase in pressure shifts diastolic peak of PPG down as decreased light absorption occurs and pressures greater than systolic pressure diminish blood flow resulting in decreased PPG amplitude (b). Effects of changes in PPG signal on amplitude.

Fig. 5.2 shows that SpO_2 and HR errors for all pressure regions are relatively constant. Furthermore, mean absolute errors are below the specified accuracy of the device, indicating that the pressure regions defined do not affect the ability to accurately measure SpO_2 and HR. A one-way ANOVA further validated that measurement accuracy is not affected by pressures ranging from 30 - 300 mmHg. This was expected since a PPG signal was identifiable for all pressure regions, indicating that vasculature occlusion did not occur. Furthermore, measurement of SpO_2 and HR when minimal noise is present is independent of the PPG amplitude. The normalization of the raw R and IR signals eliminate the dependence on PPG amplitude and the extraction of HR information depends on the quality rather than the amplitude of the PPG signal.

The extent to which SpO_2 and HR error is minimized when operating in the optimal contact pressure is shown in Fig. 5.3. When securing the sensor with a contact pressure of 30 mmHg, which is lower than the optimal pressure shown in Fig. 5.1, it was determined that the mean percentage of dropouts along with SpO_2 and HR errors are the greatest compared to securing the sensor within the optimal pressure range. The increased measurement error and reduced reliability when operating at contact pressures below the optimal range may be due to the inability to keep the sensor in close contact with the skin during walking, resulting in frequent sensor displacement for the original location and/or decoupling from the skin.

Fig. 5.3 shows that when securing the sensor with a contact pressure of 200 mmHg, which is greater than the optimal pressure range, the mean SpO_2 and HR error is slightly increased and reliability is decreased as compared to operating in the optimal contact pressure range, although the differences are not statistically significant.

Since a contact pressure of 200 mmHg still provides an identifiable PPG signal from which accurate measurements can be obtained, as verified in Fig. 5.2, measurement errors due to vessel constriction can be considered negligible. Therefore, the factor influencing the magnitude of measurement errors is SNR, as it is assumed that the degree of motion artifacts present in the signals were approximately equal since each individual walked at the same pace. Also, since statistical analysis concluded there is no significant difference in error for 80 mmHg vs. 200 mmHg, the improvement in SNR is not great enough to improve error by operating in an optimal contact pressure range. Furthermore, since normalized PPG amplitudes at 200 mmHg are less than those observed at 30 mmHg, the main source of motion artifact can be attributed to frequent sensor movement.

6.1.2. Sensor Attachment Methods

Fig. 5.4 - 5.6 shows that sensor attachment by an elastic band, adhesive tape, or integration into a helmet provides identifiable PPG signals after 10 hr. hikes, indicating that each attachment method can keep the sensor secured to the forehead over extended periods of physical activity. To further validate this observation, statistical analysis of resting SpO_2 and HR measurement errors throughout the preliminary field studies, shown in Fig. 5.7, indicate that there is no statistical difference in errors. Furthermore, all errors are within the specified accuracy of the device. Therefore, it can be concluded that all three attachment methods possess the required attribute of keeping the sensor properly secured after extended periods of physical activity.

Fig. 5.8 and Table 2 summarize how measurement accuracy and reliability during walking can be affected when each housing is utilized. The data shows that the elastic headband significantly improves measurement accuracy and reliability. This can be attributed to several factors. Firstly, because the helmet is heavy, any slight movement would cause the helmet to move. Since the sensor was attached to the helmet, it is prone to frequent movement about the forehead, which can result in motion artifacts and decrease measurement accuracy. Secondly, a tight seal is hard to achieve between the sensor and the adhesive tape. The lack of a tight seal results in a greater chance of sensor movement during walking. Also, as shown previously, contact pressure has an affect on accuracy. The contact pressure was hard to control with the adhesive tape. However, typical pressures were around 50 mmHg, slightly below the optimal pressure range. Contact pressures for the helmet were easier to control. However, pressures were around 180 mmHg as greater pressures were needed to secure the helmet properly. Contact

pressures for the elastic band were primarily on the high side of the optimal range, around 80 mmHg.

Also note that, various size heads will stretch the elastic band to varying lengths. This stretching can result in contact pressure variations between subjects, as pressure is defined as:

$$P = \frac{2T}{DW} \tag{5}$$

where,

P contact pressure

T tension

D diameter of the elastic band

W width of the elastic band.

Therefore, for an elastic band that exhibits a constant Young's modulus, the contact pressure will not vary as much with changes in head diameters. It should be mentioned that elastic bands can be designed to exhibit this property, demonstrated in previous studies, as shown in Fig. 6.3, where after 4% strain, the slope of the curve decreases to 1/15 of the original slope [64].

Also, Mannheimer et al [65] described a headband that consists of an elastic and non-elastic portion. The elastic portion is sized to fit around the subject's head, while the smaller non-elastic segment is attached to the elastic segment. The non-elastic segment is sized to span a portion of the elastic portion when it is stretched, but it is longer than the elastic segment when the elastic is not stretched. This may allow for better control of contact pressure for varying head sizes.

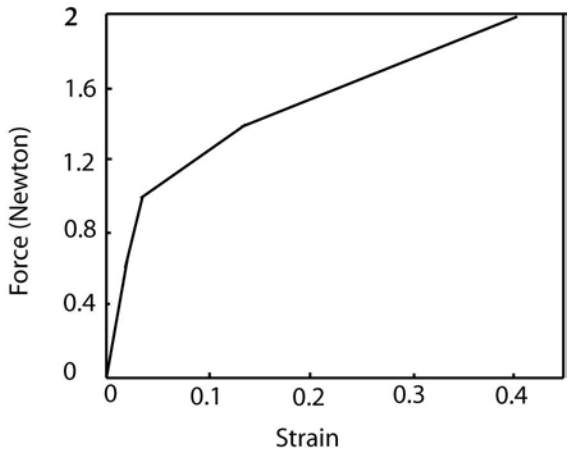

Figure 6.2. Experiment of tension-strain characteristics an elastic band redrawn from Teng [64].

6.2. Specific Aim 2 - Effects of Housing Options

The data in Fig. 5.9 shows that the normalized PPG amplitude decreases rapidly when the control housing, which represents current technology, was used. This sharp decrease can be attributed to immediate vasculature constriction resulting in decrease blood flow. Although vasculature constriction occurs, blood volume fluctuations distal to the sensor can still be detected, which explains the presence of a PPG signal in the presence of pressures greater than systolic pressure, which is generally around 120 mmHg in the suborbital artery (an artery near the sensor) [66]. At greater pressures around 1200 mmHg, the amplitude approaches a steady state value of approximately 0.1. Inspection of the signal at this pressure level shows a fluctuating signal that does not resemble a PPG. These fluctuations can be attributed to physiological and electronic noise which increases SpO_2 and HR errors, as shown in Fig. 5.10 and 5.11.

It was found that for both Housing 1 and 2, the amplitude decreased more gradually and remained at a higher value throughout the pressure range investigated, as shown in Fig. 5.9. Kruskal-Wallis one-way ANOVA on ranks verified that implementation of Housing 1 and 2 results in larger PPG amplitudes, as summarized in

Table 3 and 4. This verifies that isolating the sensor from external pressures and providing regions for blood flow to the sensor helps to maintain blood supply underneath the sensor. The tests also concluded that there is no significant different in amplitudes for Housing 1 vs. Housing 2. This was expected as each housing was designed by utilizing the same principle of isolating the sensor from pressure disturbances while maintaining blood supply to the sensor through the use of blood flow channels.

Theoretically, minimal amplitude reduction should have been observed for both Housing 1 and 2. Some reduction was expected as it is inevitable that some vasculature will become occluded. However, Fig. 5.1 shows a noticeable reduction in amplitude for both housings. This may be attributed to the design of the blood flow channels. For some subjects with a more pronounced forehead curvature, the surfaces of the two longest blood flow channels made contact with the skin when the outer-shell was displaced into the tissue, leading to vasculature constriction around the perimeter of the outer-shell. Furthermore, it was noted that the shortest blood flow channels, parallel to the headband slot, did not make contact with the skin, thus vasculature constriction did not occur in these regions, which explains why noticeable PPG signals were identified for all pressures.

To further improve the housing designs, two options can be pursued. The first is to shorten the length of the long blood flow channels so that they do not make contact with the skin for individuals with more rounded foreheads. However, this may not solve the problem because the contact area of the outer-shell is increased, thus increasing the number of blood vessels that can become occluded. The second option would be to design the housing with a flexible molded plastic so that the housing would better

conform to the subject's forehead. Although flexible, the material should provide enough strength as to not collapse when large external pressures are exerted.

Fig. 5.10 shows that SpO_2 error, for Housing 1 and 2, at pressures greater than 301 mmHg, are much less than the errors observed for the control housing due to the improved blood supply. Statistical analysis summarized in Table 3 verifies that implementation of Housing 1 and 2 results in decreased SpO_2 measurement error at pressures greater than 301 mmHg. Especially important is that SpO_2 error is improved in the region of 600 - 1200 mmHg, which represents typical pressures applied to the sensor should an injured individual fall on the sensor. Furthermore, Fig. 5.11 shows that HR error, for Housing 1 and 2, at pressures greater than 301 mmHg are less than the errors observed for the control housing to the improvement of blood supply to the sensor. Statistical analysis of all observed HR errors concluded that the two new housings vs. the control result in improved HR accuracy for any pressures greater than 601 mmHg.

The improvement in SpO_2 and HR accuracy for the newly designed housings was expected due to the lack of an identifiable PPG signal from the control housing in the presence of large pressures. This improvement is especially important for a situation where a soldier is wounded and falls on the sensor. For this situation, a pressure as high as 1200 mmHg could be applied to the sensor. If the current technology or control housing is used, measurement error due to the lack of a PPG signal can be as high as 23 % O_2 or 31 bpm, however, Housing 1 or 2 can provide mean measurement errors of 3 % O_2 and 4 bpm, as shown in Fig. 5.10 and 5.11. It should also be noted that the reported errors for the control housing may be misrepresentative. Since there was no identifiable PPG signal in the presence of large pressures, SpO_2 and HR cannot be measured and

therefore the error can be considered infinite. Finite measurement errors of 23 % and 31 bpm can be attributed to past data averaging by the pulse oximeter of sections of the signal containing data that could be mistaken as a PPG signal. Nevertheless, the decision not to report the errors as infinite were chosen based on the assumption that PPG, SpO_2, and HR data will most likely not be seen by a medic, but rather used by a microprocessor to place the subject in a triage category, an issue being researched [67].

Statistical analysis of the normalized PPG amplitude data shown in Fig. 5.9 and SpO_2 and HR error shown in Fig. 5.10 and 5.11, respectively, did not conclude that there is a statistically significant difference between Housing 1 and 2. This was expected as each housing functioned on the same principle, which was to keep the sensor in contact with the skin at a constant pressure while preventing vascular collapse under the sensor. Nevertheless, based on the data presented, this isolating principle has shown to provide larger PPG amplitudes and decreased SpO_2 and HR error in the presence of large vessel constricting pressures which may occur during RPSM.

7. Future Recommendations

Despite the advantages of reflectance pulse oximetry for RPSM, motion and pressure artifacts can lead to inaccurate measurement of physiological variables. Although motion artifacts cannot be completely eliminated, for pulse oximetry to become a viable means for use with RPSM, artifacts must be reduced to the extent where measurement error is within the clinically accepted range. To further reduce artifact related measurement errors beyond that achieved by previous studies, research aimed at determining the effects of various sensor housing and attachment methods was conducted.

The results indicate that the pressure used to secure a pulse oximeter sensor to the forehead plays a pivotal role in the ability to accurately measure SpO_2 and HR during walking. Contact pressures should be greater than 30 mmHg to reduce chances of sensor displacement about the skin. Pressures greater than 300 mmHg should also be avoided as vasculature constriction leads to increased measurement error. Data also suggests that contact pressures ranging from 60 – 80 mmHg are optimal. In the interest of user acceptability, the low end of this pressure region should be utilized for improved comfort over extended periods of time. Further research should be conducted to determine if pressures ranging from 30 – 60 mmHg provide the same measurement accuracy during walking, as these lower pressures are more optimal for user-acceptability.

The data indicated that the method used to attach a pulse oximeter sensor to forehead can impact the ability to accurately measure SpO_2 and HR. A method that attaches the sensor to a heavy mass, such as helmet, should be avoided to reduce the chance of sensor displacement about the skin. An adhesive tape should also be avoided as frequent sensor displacement, leading to increased measurement error, can occur. An

attachment method that is flexible to conform to the forehead, yet provides sufficient contact pressure greater than 30 mmHg, such as an elastic headband, was shown to significantly improve measurement error and reliability. If this attachment method is used, a band having a constant strain/tension relationship can provide constant contact pressures despite various size heads.

Despite having an attachment method that provides an optimal contact pressure, the possibility exists that a large pressure will be applied to the sensor, when a soldier is injured and falls on it. With current technologies, it was shown that these large pressures lead to unacceptable SpO_2 and HR errors. To overcome these effects, two new housings operating on the same principle were designed. Each housing isolates the pulse oximeter sensor from large pressure disturbances and keeps the vasculature network around the sensor unperturbed so that blood supply can be maintained. The results indicated that the principle employed for sensor isolation can significantly decrease SpO_2 and HR errors in the presence of large pressure disturbances. Although both housings showed significant error improvement, housings based on the same principle but conform to the subject's forehead should be developed and studied as measurement errors may be further reduced.

Although this research has provided evidence that the use of an elastic band providing 60 mmHg of contact pressure combined with an isolating sensor housing can significantly reduce measurement errors due to the reduction of motion and pressure artifacts, the presence of artifact related errors still exist. Because activities other than walking will introduce different degrees of motion artifacts, research should be conducted on the measurement accuracy of the sensor mountings studied during activities users of the device would encounter to further validate the conclusions of this thesis.

8. REFERENCES

1. The American Telemedicine Association, "Defining Telemedicine," [Online white paper], (2005), [2005 Aug 31], Available at HTTP: http://www.atmeda.org/news/definition.html.
2. Lynch JP, "Overview of Wireless Sensors for the Real-Time Health Monitoring of Civil Structures," *Proc. of the 4th International Workshop on Structural Control and Monitoring*, New York, NY, June 10-11, 2004.
3. Malan D, et al., "CodeBlue: An Ad Hoc Sensor Network Infrastructure for Emergency Medical Care", *International Workshop on Wearable and Implantable Body Sensor Networks*, Apr. 2004.
4. Friedl KE, Allan JH, "USARIEM: Physiological Research for the Warfighter", *Army Medical Department Journal*, 4Q, 2004.
5. Anliker U, et al., "AMON: A Wearable Multiparameter Medical Monitoring and Alert System", *IEEE Transactions on Information Technology in Biomedicine*, 8(4), 2004.
6. Ling G, et al., "In Search of Technological Solutions to Battlefield Management of Combat Casualties," *Proc. of the SPIE Conference on Battlefield Biomedical Technologies*, 3712, pp. 1-8, July 1999.
7. Seth G, et al., "Establishing Law and Order After Conflict," RAND Corporation, Santa Monica, CA, 2005.
8. Mendelson Y, Nagre A, Dresher R "The Feasibility of Measuring SpO_2 from the Head Using a Reflectance Pulse Oximeter: Effect of Motion Artifacts," *Proc. of the 3rd European Medical & Biological Engineering Conference*, Prague, Czech Republic, Nov. 2005.
9. Kremens R, Faulring J, Phillips D, "A Compact Device to Monitor and Report Firefighter Health, Location, and Status," *8th International Wildland Fire Safety Summit*, Missoula, MT, Apr. 26-28, 2005.
10. Asada H, et al., "Mobile Monitoring with Wearable Photoplethysmographic Biosensors," *IEEE Engineering in Medicine and Biology Magazine*, 22(3), pp. 28-40, 2003.
11. Park S, Jayaraman S, "Enhancing the Quality of Life through Wearable Technology," *IEEE Engineering in Medicine and Biology Magazine*, 22(3), pp. 41-8, 2003.
12. Aoyagi T, "Pulse oximetry: its invention, theory, and future," *Journal of Anesthesia*, 17, pp. 259-66, 2003.
13. Crilly PB, et al., "An Integrated Pulse Oximeter System for Telemedicine Applications," *Proc. of the IEEE Instrumentation and Measurements Technical Conference*, Ottawa, Canada, May 19-21, 1997.
14. Kamat V, "Pulse Oximetry," *Indian Journal of Anesthesia*, 46(4), pp. 261-8, 2002.
15. Mendelson Y, "Pulse Oximetry: Theory and Applications for Noninvasive Monitoring," *Clinical Chemistry*, 38(9), pp. 1601-7, 1992.
16. Mendelson Y, Pujary C, Savage M, "Minimization of LED Power Consumption in the Design of a Wearable Pulse Oximeter," *Proc. of the IASTED International Conference of Biomedical Engineering*, pp. 249-54, Salzburg, Austria, June 25-27, 2003.

17. Johnston W, Mendelson Y, "Extracting Heart Rate Variability from a Wearable Reflectance Pulse Oximeter," *Proc. of the 31st Annual IEEE Northeast Bioengineering Conference*, Hoboken, NJ, April 2005.
18. Rusch TL, Sankar R, Scharf JE, "Signal Processing Methods for Pulse Oximetry," *Computers in Biology & Medicine*, 26(2), pp. 1430-59, 1996.
19. Zamarron C, et al., "Utility of Oxygen Saturation and Heart Rate Spectral Analysis Obtained from Pulse Oximetric Recordings in the Diagnosis of Sleep Apnea Syndrome," *Chest Journal*, 123(5), pp. 1567-76, 2003.
20. Konig V, Huch R, Huch A, "Reflectance Pulse Oximetry-Principles and Obstetric Application in the Zurich System," *Journal of Clinical Monitoring and Computing*, 14(6), pp. 403-12, 1998.
21. Illustration by Nicole Cavenas.
22. Nonin Medical Inc., "Avant 4000," [Online product brochure], 2005, [Apr 16 2005], Available at HTTP: http://www.nonin.com/products/4000.asp.
23. Mendelson Y, Ochs BD, "Noninvasive Pulse Oximetry Utilizing Skin Reflectance Photoplethysmography," *IEEE Transactions on Biomedical Engineering*, 35(10), pp. 798-805, 1988.
24. Ezri T, et al., "Pulse Oximetry from the nasal septum," *Clinical Anesthesia*, 3(6), pp. 447-50, 1991.
25. Lema GE, "Oral Pulse Oximetry in Small Children," *Anesthesia & Analgesia*, 72(3), pp. 414, 1991.
26. Robertson RE, Kaplan RF, "Another Site for the Pulse Oximeter Probe," *Anesthesiology*, 74(1), pp. 198, 1991.
27. Palve H, "Comparison of Reflection and Transmission Pulse Oximetry after Open Heart Surgery," *Critical Care Medicine*, 20(1), pp. 48-51, 1992.
28. Chaffin MK, et al., "Evaluation of Pulse Oximetry in Anesthetized Fouls Using Multiple Combinations of Transducer Type and Transducer Attachment Site," *Equine Veterinary Journal*, 28(6), pp. 437-45, 1996.
29. Dassel C, "Experimental Studies on Reflectance Pulse Oximetry: Specific Aspects of Intrapartum Fetal Monitoring," [thesis], University of Groningen, 1997.
30. Gehring H, et al., "The Effects of Motion Artifact and Low Perfusion on the Performance of a New Generation of Pulse Oximeters in Volunteers Undergoing Hypoxemia," *Respiratory Care*, Jan. 2002.
31. Palve H, "Reflection and Transmission Pulse Oximetry during Compromised Peripheral Perfusion," *Clinical Monitoring*, 8(1), pp. 12-5, 1992.
32. Miyai N, et al., "Preliminary Study on the Assessment of Peripheral Vascular Response to Cold Provocation in Workers Exposed to Hand-Arm Vibration Using Laser Doppler Perfusion Imager," *Industrial Health*, 43, pp. 548-55, 2005.
33. Johnston WS, et al., "Effects of Motion Artifacts on Helmet-Mounted Pulse Oximeter Sensors," *Proc. of the IEEE 30th Annual Bioengineering Conference*, pp. 214-5, 2004.
34. Webb RK, Ralston AC, Runciman WB, "Potential Errors in Pulse Oximetry. II. Effects of Changes in Saturation and Signal Quality," *Anesthesia*, 46(3), pp. 207-12, 1991.
35. Hatlestad D, "Revolution in Pulse Oximetry Enhances Respiratory Patient Care," *The Journal for Respiratory Care Practitioners*, Oct/Nov 2001.

36. Nogawa M, Kaiwa T, Takatani S, "A Novel Hybrid Reflectance Pulse Oximeter Sensor with Improved Linearity and General Applicability to Various Portions of the Body," *Proc. of the 20th Annual International Conference of the IEEE Engineering in Medicine and Biology Society*, 20(4), pp. 1858-61, 1998.
37. Bebout DE, Mannheimer PD, "Detection of Hypoxemia During Peripheral Vasoconstriction at the Radial Artery and Various Pulse Oximeter Sensor Sites," *Critical Care Medicine*, 31(2):A72, 2003.
38. Mendelson Y, Pujary C, "Measurement Site and Photodetector Size Considerations in Optimizing Power Consumption of a Wearable Reflectance Pulse Oximeter," *Proc. of the 25th Int. IEEE EMBS Conference*, Cancun, Mexico, Sept. 2003.
39. Sugino S, et al., "Forehead is as Sensitive as Finger Pulse Oximetry during General Anesthesia," *Canadian Journal of Anesthesia*, 51(5), pp. 432-6, 2004.
40. Dassel, C, et al., "Reflectance Pulse Oximetry at the Forehead Improves by Pressure on the Probe," *Journal of Clinical Monitoring*, 11(4), pp. 237-44, 1995.
41. Dassel C, et al., "Reflectance Pulse Oximetry at the Forehead of Newborns. The influence of varying pressure on the probe," *Journal of Clinical Monitoring*, 12(6), pp. 421-8, 1996.
42. Teng XF, Zhang YT, "The Effect of Contacting Force on Photoplethysmographic Signals," *Physiological Meas*urement, 25, pp. 1323-35, 2004.
43. Dresher R, Mendelson Y, "Attachment of a Wearable Skin Reflectance Pulse Oximeter," *Proc. of the 2005 BMES Annual Fall Meeting*," Baltimore, MD, Sept 28 - Oct 1, 2005.
44. Rhee S, Yang B-H, Asada HH, "Design and Evaluation of Artifact-Resistant Finger-Ring Plethysmographic Sensors," *Proc. of the ASME International Mechanical Engineering Congress & Exposition*, Orlando, FL, Nov. 5-10, 2000.
45. Sola A, Chow L, Rogido M, "Pulse Oximetry in Neonatal Care. A Comprehensive State of the Art Review," *Anales of Pediatria*, 62(3), pp. 266-80, 2005.
46. Hayes MJ, et al., "Quantitative Investigation of Artefact in Photo-plethysmography and Pulse-Oximetry for Respiratory Exercise Testing," *Proc. of the CNVD 97 Frontiers in Computer-Aided Visualization of Vascular Functions*, pp. 117-24, 1998.
47. Hayes MJ, Smith PR, "Artifact Reduction in Photoplethysmography," *Applied Optics*, 37(31), pp. 7437-46, 1998.
48. Hayes MJ, Smith PR, "A New Method for Pulse Oximetry Possessing Inherent Insensitivity to Artifact," *Proc. of the IEEE Transactions on Biomedical Engineering*, 48(4), 2001.
49. Yan Y, Poon CC, Zhang Y, "Reduction of Motion Artifact in Pulse Oximetry by Smoothed Pseudo Wigner-Ville Distribution," *Journal of Neuroengineering and Rehabilitation*, 2(3), 2005.
50. Coetzee FM, Eighazzawi Z, "Noise-Resistant Pulse Oximetry Using a Synthetic Reference Signal," *Proc. of the IEEE Transactions on Biomedical Engineering*, 47(8), pp. 1018-26, 2000.
51. Barker S, Morgan S, "A Laboratory Comparison of the Newest "Motion Resistant" Pulse Oximeters during Motion and Hypoxemia," *Anesthesia and Analgesia*, 95(55), S2:A6, 2004.
52. Barker S, "The effect of Motion of the Accuracy of Six Motion-Resistant Pulse Oximeters," *Anesthesiology*, 95:A586, 2001.

53. Rhee S, Yang B-H, Asada HH, "Artifact-Resistant Power-Efficient Design of Finger-Ring Plethysmographic Sensors," *IEEE Transactions on Biomedical Engineering*, 48(7), pp. 795-805, 2001.
54. Dassel C, et al., "Effect of Location of the Sensor on Reflectance Pulse Oximetry," *British Journal of Obstetrics and Gynaecology*, 104, pp. 910-6, 1997.
55. Nagre A, Mendelson Y, "Effects of Motion Artifacts on Pulse Oximeter Readings from Different Facial Regions," *Proc. of the IEEE 31st Annual Northeast Bioengineering Conference*, pp. 220-222, 2005.
56. Mannheimer PD, et al., "The Influence of Larger Subcutaneous Blood Vessels on Pulse Oximetry," *Journal of Clinical Monitoring*, 18, pp. 179-88, 2004.
57. Nonin Medical Inc., "Pure Light," [Online product brochure], 2005, [Jun 17 2005], Available at HTTP: http://www.nonin.com/documents/PureLight%20Sensors%20Brochure.pdf.
58. Cooke JE, Scharf JE, "Forehead Pulse Oximetry in the Trendelenberg Position," *Proc. of the Annual Fall Meeting of the American Society of Anesthesiologists*, Chicago IL, Oct 2006.
59. Nellcor Puritan Bennet Inc. [Website], 2006, [Apr 28 2006], Available at HTTP: http://www.nellcor.com.
60. Shelley K, et al., "The Effect of Venous Pulsation on the Forehead Pulse Oximeter Wave Form as a Possible Source of Error in SpO_2 Calculation," *Anesthesia & Analgesia*, 100, pp. 743-7, 2005.
61. Rhee S, Yang B-H, Asada HH, "Theoretical Evaluation of the Influence of Displacement on Finger Photoplethysmography for Wearable Health Monitoring Sensors," *Symposium on Dynamics, Control, and Design of Biomechanical Systems ASME International Mechanical Engineering Congress and Exposition*, Nashville, TN, Nov 1999.
62. Vegors M, Lindberg LG, Lennmarken C, "The Influence of Changes in Blood Flow on the Accuracy of Pulse Oximetry in Humans," *Acta Anaesthesiologica Scandinavica*, 36(4), pp. 346-9, 1992.
63. Rhee S, Yang B-H, Asada HH, "Artifact Resistant, Power-Efficient Design of a Finger-Ring Plethysmographic Sensors, Part I: Design and Analysis," *Proc. of the 22nd Annual International Conference of the IEEE Engineering in Medicine and Biology Society*, Chicago, IL, Jul. 2000.
64. Rhee S, Yang BH, Asada HH, "Design of a Artifact-Free Wearable Plethysmographic Sensor," *Proc. of the 21st Annual International Conference of the IEEE EMBS*, Atlanta, GA, Oct. 1999.
65. Mannheimer PD, et al., "Forehead Sensor Placement," US Patent Application 10,678,040, To Nellcor Puritan Bennett Incorporated, Patent and Trademark Office, 2003.
66. Lee TK, Westenkow DR, "Comparison of Blood Pressure Measured by Oscillometry from the Suborbital Artery and Invasively from the Radial Artery," *Journal of Clinical Monitoring & Computing*, 14(2), pp. 113-7, 1998.
67. Knorr BR, "Using Neural Networks to Identify Airway Obstructions in Anesthetized Patients Based on Photoplethysmograph," *Proc. of the 32nd Annual IEEE NEBEC*, Easton, PA, Apr. 2006.

Appendix A - Preliminary Data of Optimal Contact Pressure Study

Fig. A.1 shows the observed effects of contacting force on normalized AC amplitude. The data was used to determine an appropriate sample size for the final investigation of contact pressure on PPG amplitude.

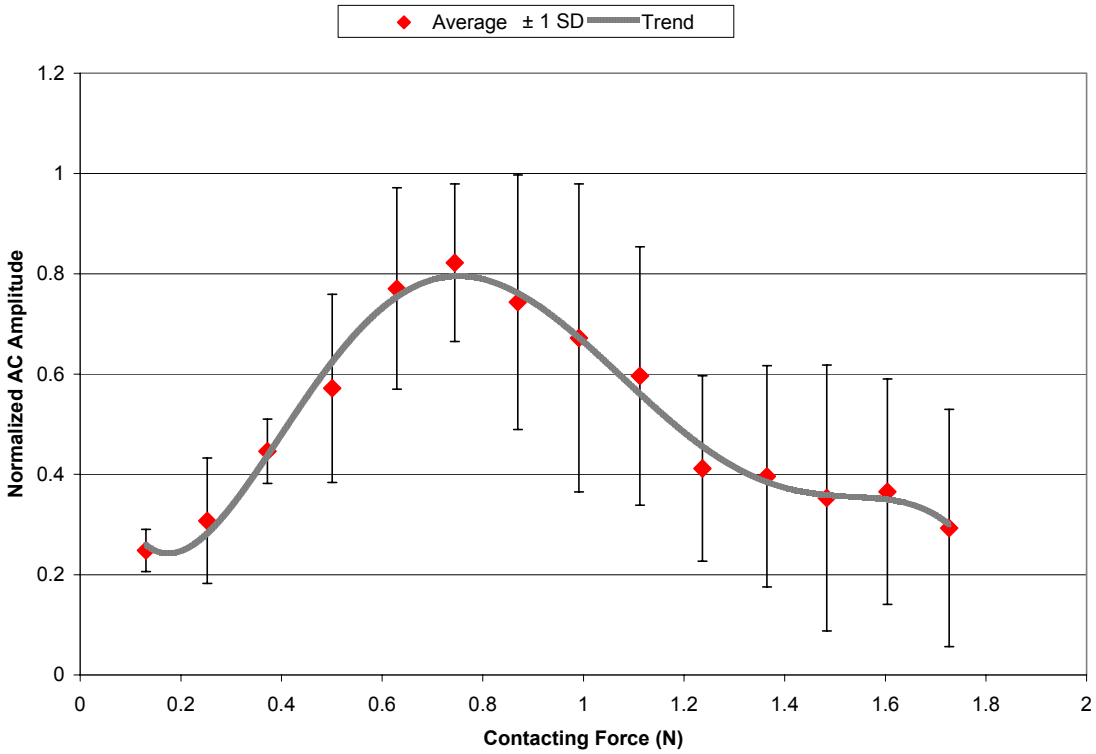

Figure A.1. Preliminary measurements for effects of contacting force on AC amplitude.

Appendix B - LabVIEW Programs for Recording SpO_2, HR, and PPG Data from Nonin Sensors

The following LabVIEW programs were used in both the optimal contact pressure range study and the sensor housing investigation. Fig. B.1 shows the main program used to record SpO_2, HR, and PPG data from the Nonin™ sensor. The components to the left of the error block (1) initialize the system for serial data retrieval. If there are no errors, the data is indexed into an array by the components below the error block. The indexed array contains the bytes from the sensor, and defines these bytes as local variables which are called to the right of the error block. Fig. B.2 - B.6 show the alternate cases for the case structures labeled by large red font in Fig. B.1. If there is an error in data retrieval from the sensors, the error block shown in Fig. B.2. stops the program and displays the error code for troubleshooting. Because the data from the sensor and Xpod comes in byte by byte, the case structure shown in Fig. B.3 outputs the current byte to the correct variable. The first byte or case shown in Fig. B.1 corresponds to the most significant bit for heart rate, the case in Fig. B.3a corresponds to the least significant bit for heart rate, Fig. B.3b corresponds to SpO_2, and Fig. B.3c corresponds to a revision number. Since no new data is contained when the revision number is read, the previous values of SpO_2 and HR are outputted. In order to properly determine the current byte, the case structure labeled as 3 is used. This checks to see if the status byte is equal to 129, which corresponds to the most significant byte of HR. Knowing this is true, the case structure labeled 2 can function properly. If the status byte does not equal 129, the alternate case of 3 shown in Fig. B.4 is implemented, which waits for the status byte to equal 129. Blocks 4 - 7 and the alternate cases shown in Fig. B.5 combine the most and least significant HR bytes to yield the correct heart rate. The status byte also contains information about the signal,

such as if it is a bad pulse, there is low perfusion, or the sensor is disconnected. This information is encoded in bit form and is defined in the green components underneath block 3 in Fig. B.1. The program will set SpO_2 to zero should the sensor be disconnected, the pulse is out of track or a bad pulse is encountered. This is accomplished by blocks 8 through 12 and their alternate cases depicted in Fig. B. 6. PPG HR and SpO_2 from the Nonin sensor are outputted by this program.

The sensor reading program of Fig. B.1 is called by the sub-function, Nonin Xpod®, of the program illustrated in Fig. B.7. The program also acquires pressure data from the load cell and records all data to one text file. The upper most components shown in orange correspond to force acquisition from the load cell. The components outside the loop initialize the system for analog measurement from the DAQ module. The data is filtered with a low pass filter and then converted to pressure by the mathematical components. A pressure null component is provided so the user can zero out the pressure. The data is then indexed into an array. The components on the second line create a .txt file where the pressure data is saved to, and writes the data to the file in the case structure labeled as 1. If the user does not wish to save the data to the file, the case structure resorts to its alternate case shown in Fig. B.8, which does not write data to file. The components below this case structure serve read the sensor data outputted from the program in Fig. B.1 and indexes the data into an array where it is written to a .txt file by the case structure labeled as 2. Note that to function properly, the two Nonin Xpod® sub-functions in Fig. B.7 must be two different files.

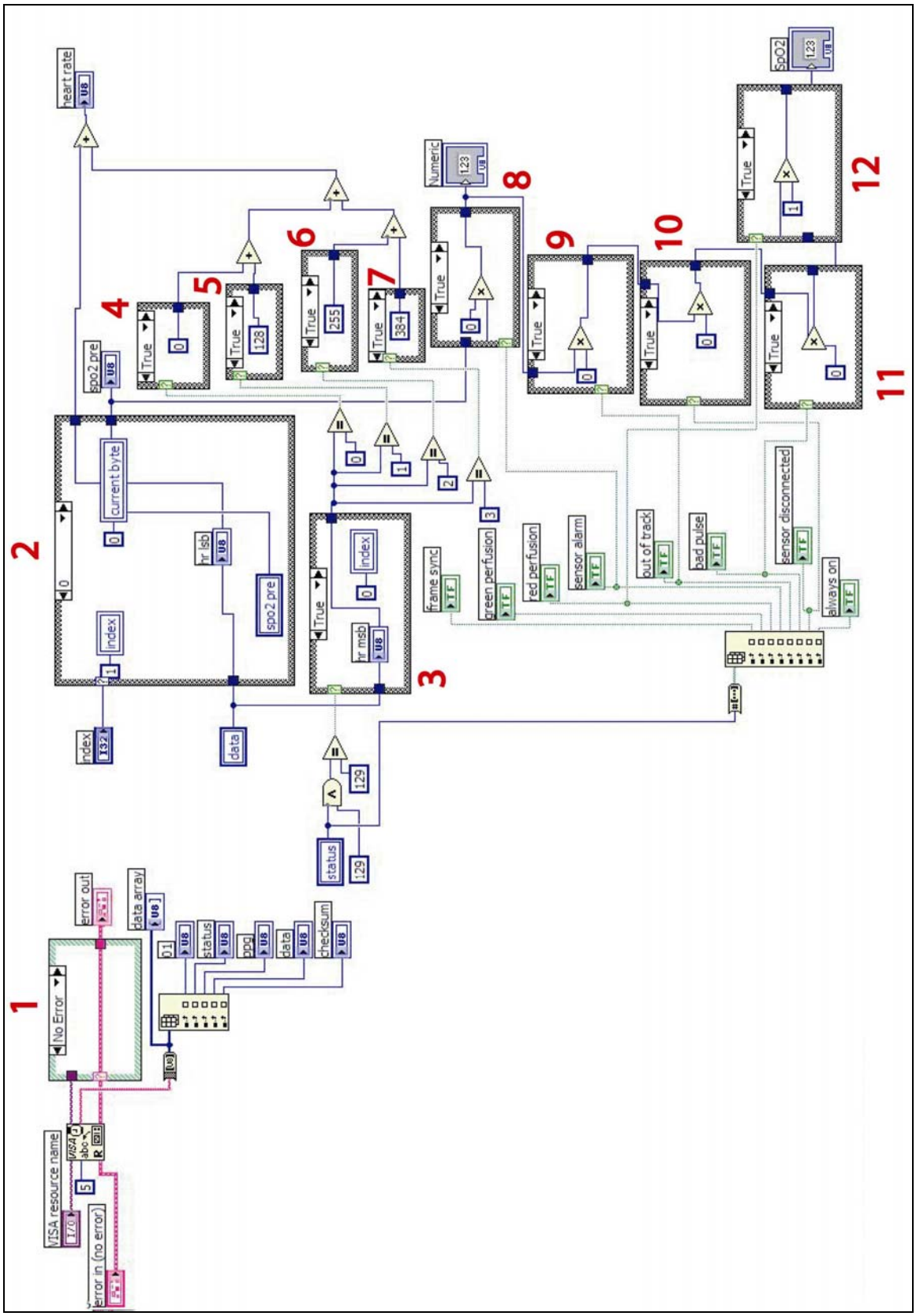

Figure B.1. LabVIEW program for recording of Nonin data.

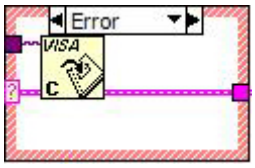

Figure B.2. Alternate case for the error handling block (1).

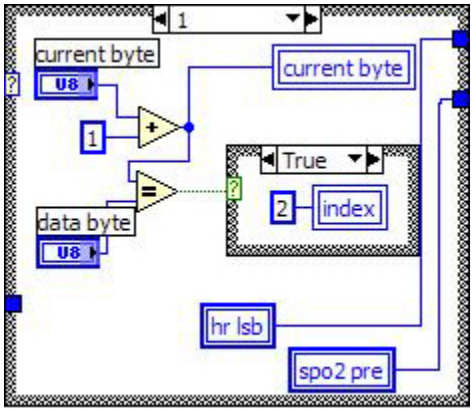

a.

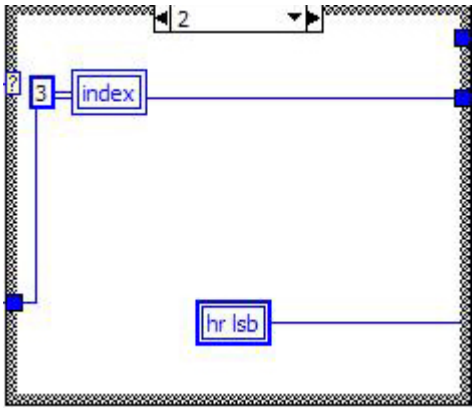

b.

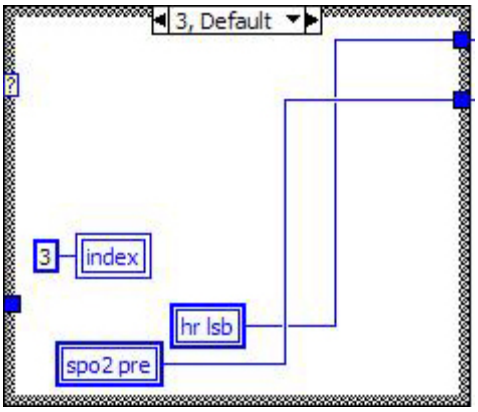

c.

Figure B.3. Alternate cases for the read block (2).

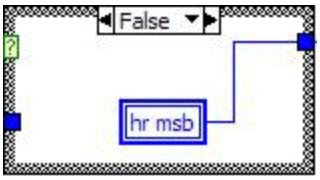

Figure B.4. Alternate case for initializing measurement block (3).

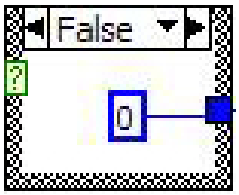

Figure B.5. Alternate case for HR measurement blocks (4 - 7).

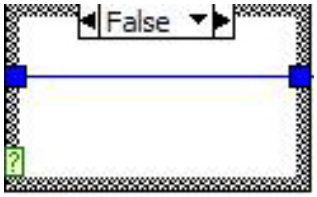

Figure B.6. Alternate case for SpO_2 measurement blocks (8 - 12).

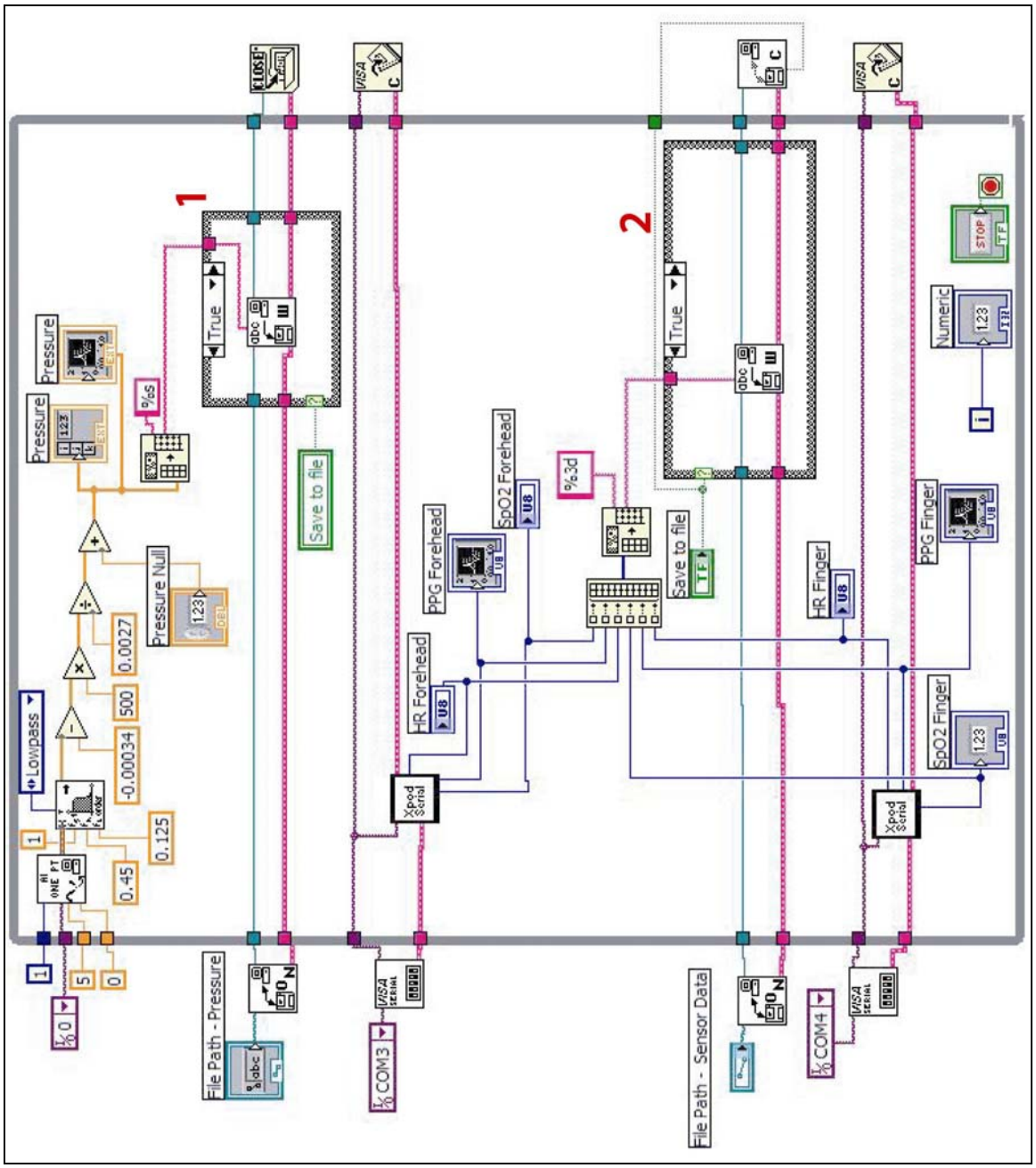

Figure B.7. LabVIEW program used for pressure studies.

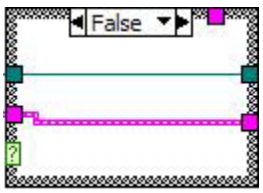

Figure B.8. Alternate case for data writing blocks (1, 2).

Appendix C - MATLAB Program for Calculation of PPG Amplitude and Resting Measurement Errors

The following MATLAB code was used for both the optimal contact pressure study and housing investigation. It is to be used in conjunction with LabVIEW programs of Appendix A. The program calculates the average peak-to-peak amplitude of a PPG waveform, SpO_2 and HR errors between the 2 sensors, for varying pressure levels measured from the load cell. Note that all green text is comments.

```
To be used with the Nonin pulse oximeter and Xpod and MSI compressive load cell

Loads pressure, PPG, SpO2, and HR data for both sensors
Prompts user for .txt file where data is saved to
tdfread;
Takes third column of data and assigns that as Forehead PPG data.  If the forehead PPG
data is in a different column besides 3, change the number 3 after the underscore to the
correct column
ForeheadPPG=tdfread_3;
The rest of the functions below are the same as the above line of code
ForeheadSpO2=tdfread_2;
ForeheadHR=tdfread_4;
FingerSpO2=tdfread_5;
FingerHR=tdfread_7;
FingerPPG=tdfread_6;
Pressure=tdfread_8;

Calculate PPG amplitude of forehead sensor for each pressure level
Sets positive and negative peak threshold to 100, so false peaks are not detected
PositivePeakThreshold=100;
NegativePeakThreshold=100;
Prompts the user for the number of pressure ranges contained in the data set.
NumberofPressureRanges=input('Number of Pressure Range? ');
Determines the ending data point for each pressure range studied by asking the user the
ending point, which is accomplished in the 3rd line of code below
i=1;
while i<=NumberofPressureRanges-1
   EndofPressureRange(i)=input('End of Pressure Range? ');
   i=i+1;
end
```

```
LPF to smooth out PPG signal
2nd order LPF with 25 Hz cutoff
[B,A] = butter (2,.05);
Y = filter(B,A,ForeheadPPG);

Positive peak detection loop using for loop to span the entire signal
count = 1;
for u = 2:1:(length(Y))-1;
Takes first derivative of PPG signal
   r = diff(Y);
Positive peak detection by detecting change in sign of slope and also compares the peak
to the threshold set above so false peaks are not detected.  Stores the location of each
peak
   if r(u - 1) > 0 & r(u) <= 0 & Y(u) > PositivePeakThreshold
      u;
      peaks_index(count) = u;
      count = count + 1;
   end
end

Positive spline calculation used to connect the detected positive peaks, which forms the
positive envelope of the signal
x = peaks_index;
c = Y(peaks_index);
xx = [1 :length(Y)];
yy = spline(x,c,xx);

Negative peak detection loop, operates under same ideology as the positive peak
detection loop
counts = 1;
for uu = 2:1:(length(Y))-1;
   if r(uu - 1) < 0 & r(uu) >= 0 & Y(uu) < NegativePeakThreshold
      uu;
      peaks_indexs(counts) = uu;
      counts = counts + 1;
   end
end

x1 = peaks_indexs;
c1 = Y(peaks_indexs);
xx1 = [1 : length(Y)];
yy1 = spline(x1,c1,xx1);
```

```
Subtracts mean of negative envelope from mean of positive envelope to determine peak-to-peak amplitude, does this for all pressure ranges using the while loop.
i=1;
Code before the while loop determines PPG amplitude for first pressure region.  Starts the calculation at the 100th data point because initial spline transient can induce large errors.
AverageAmplitudePressure(i) = mean(yy(100:EndofPressureRange(i))) - mean(yy1(100:EndofPressureRange(i)));
i=i+1;
While loop to investigate pressure ranges from 2 to the pressure level before the last.
while i<=NumberofPressureRanges-1
   AverageAmplitudePressure(i) = mean(yy(EndofPressureRange(i-1):EndofPressureRange(i))) - mean(yy1(EndofPressureRange(i-1):EndofPressureRange(i)));
   i=i+1;
end
Determines PPG amplitude for the last pressure region.  Ends the calculation at the 100th data point before the last because the spline transient can induce large errors.
AverageAmplitudePressure(i) = mean(yy(EndofPressureRange(i-1):length(ForeheadPPG)-100)) - mean(yy1(EndofPressureRange(i-1):length(ForeheadPPG)-100));
AverageAmplitudePressure=AverageAmplitudePressure';

Determines average pressure for each pressure range inputted by the user at the beginning of the program.  This operates under the same ideology as the amplitude calculation above
i=1;
AveragePressure(i)=mean(Pressure(100:EndofPressureRange(i)));
i=i+1;
while i<=NumberofPressureRanges-1
   AveragePressure(i)=mean(Pressure(EndofPressureRange(i-1):EndofPressureRange(i)));
   i=i+1;
end
AveragePressure(i)=mean(Pressure(EndofPressureRange(i-1):length(ForeheadPPG)-100));
AveragePressure=AveragePressure';

Calculates HR and SpO2 errors for each pressure range, where error is defined as forehead - fingertip data.  Operates under the same ideology as the previous 2 sections of code
HR_differences = ForeheadHR-FingerHR;
SpO2_differences = ForeheadSpO2-FingerSpO2;
i=1;
AverageHRDifference(i)=mean(HR_differences(100:EndofPressureRange(i)));
AverageSpO2Difference(i)=mean(SpO2_differences(100:EndofPressureRange(i)));
```

```
i=i+1;
while i<=NumberofPressureRanges-1
   AverageHRDifference(i)=mean(HR_differences(EndofPressureRange(i-
1):EndofPressureRange(i)));
   AverageSpO2Difference(i)=mean(SpO2_differences(EndofPressureRange(i-
1):EndofPressureRange(i)));
   i=i+1;
end
AverageHRDifference(i)=mean(HR_differences(EndofPressureRange(i-
1):length(ForeheadPPG)-100));
AverageSpO2Difference(i)=mean(SpO2_differences(EndofPressureRange(i-
1):length(ForeheadPPG)-100));
AverageHRDifference=AverageHRDifference';
AverageSpO2Difference=AverageSpO2Difference';

Saves the calculated PPG amplitude, HR and SpO2 errors, and pressure data to .txt files
in the directory you are currently working in.  Each file contains the calculated value for
each pressure range, starting from lowest to highest pressure.
save Amplitude.out AverageAmplitudePressure -ASCII
save Pressure.out AveragePressure -ASCII
save AverageHRDifference.out AverageHRDifference -ASCII
save AverageSpO2Difference.out AverageSpO2Difference -ASCII
```

Appendix D - LabVIEW Program for Recording SpO_2 and HR During Motion

The LabVIEW program shown in Fig. D.1 was used in both the optimal contact pressure during motion study and the attachment method studies. Note that the program is exactly the same as that shown in Fig. B.7, except that it does not contain the pressure measurement and recording part that is located in the top part of Fig. B.7. Refer to Appendix B and the discussion of Fig. B.7 concerning the functioning of this program.

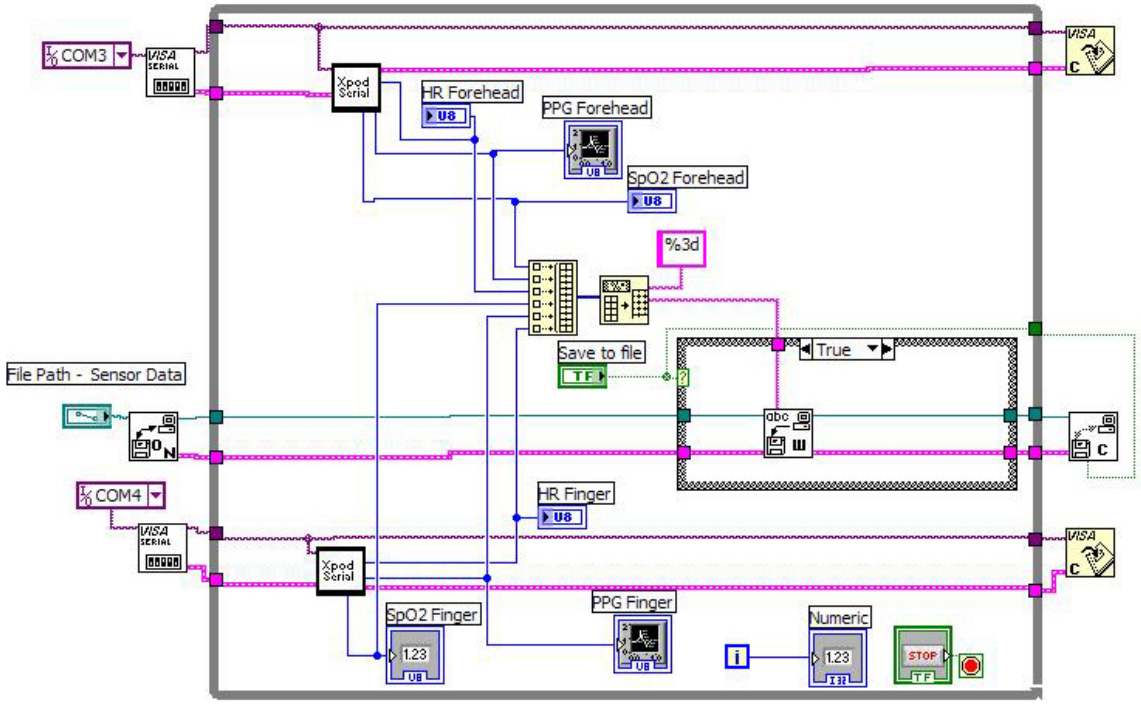

Figure D.1. LabVIEW program used for motion studies.

Appendix E - MATLAB Program for the Calculation of SpO_2 and HR Errors and Dropouts During Walking

The following MATLAB code was used for both the optimal contact pressure during motion study and the attachment method studies. It is to be used in conjunction with LabVIEW programs of Appendix C. The program calculates the mean absolute SpO_2 and HR errors, where error is defined as (forehead-fingertip) data. The program also determines and displays the number of measurement dropouts for a give time period. The number of dropouts is not factored into the measurement error. Note that all green text is comments.

```
Loads SpO2 and HR data from forehead and fingertip sensor
Promputs user for .txt file that the data is saved to
tdfread;
Assigns the second column of data to the ForeheadSpO2 variable.  If the second column
is not SpO2 data from the forehead, change the number after the underscore to the correct
column
ForeheadSpO2=tdfread_2;
Next 3 lines of code function the same way
ForeheadHR=tdfread_4;
FingerSpO2=tdfread_5;
FingerHR=tdfread_7;

Determines percentage of dropouts where dropouts are defined as SpO2 values equal to
zero or greater than 100 % and HR values equal to 0 or 255 bpm.  Prints the percentage
of dropouts on the screen
i=1;
NumberofSpO2DropOuts=0;
NumberHRDropOuts=0;
while i<=length(ForeheadSpO2)
   if (ForeheadSpO2(i)==0) || (ForeheadSpO2(i)>100)
      NumberofSpO2DropOuts=NumberofSpO2DropOuts+1;
   end
   if (ForeheadHR(i)==0) || (ForeheadHR(i)==255)
      NumberHRDropOuts=NumberHRDropOuts+1;
   end
   i=i+1;
end
PercentDropOuts=(NumberofSpO2DropOuts+NumberHRDropOuts)/length(ForeheadHR
)
```

```
Deletes SpO2 and HR dropouts from dataset
i=1;
while i<=length(ForeheadSpO2)
   if (ForeheadSpO2(i)==0) || (ForeheadSpO2(i)>100) || (ForeheadHR(i)==0) ||
(ForeheadHR(i)==255)
       ForeheadSpO2(i,:)=[];
       FingerSpO2(i,:)=[];
ForeheadHR(i,:)=[];
       FingerHR(i,:)=[];
       i=i-1;
   end
   i=i+1;
end

Calculates SpO2 and HR errors for the dataset not containing any dropouts.  Error is
defined as forehead-fingertip data.  Prints each average error on the screen
SpO2Error=ForeheadSpO2-FingerSpO2;
HRError=ForeheadHR-FingerHR;
AverageSpO2Error=mean(SpO2Error(1:length(ForeheadSpO2)))
AverageHRError=mean(HRError(1:length(ForeheadHR)))
```

Appendix F - Optimal Contact Pressure

Fig. F.1 shows typical measured PPG amplitudes at varying contact pressures. Each point on the graph represents the mean amplitude of the PPG signal. Because the commercial pulse oximeter outputs ASCII type PPG data, the mean amplitude does not have units, but is related to the ASCII values. Although all 10 individuals exhibited trends similar to that shown in the figure, the relative amplitudes for each individual were different. In order to determine the optimal contact pressure range, the variations in amplitude among individuals was eliminated by normalizing the data. This was achieved for each individual by normalizing the largest PPG amplitude to a value of one. This process served as the basis for the rest of the normalization process. Fig. F.2 shows that normalization preserves the trend shown in Fig. F.1. However, the amplitudes can only take on values from 0-1, which allows for the comparison of multiple individuals.

Because measurements were not performed at exactly the same pressure for each individual, the normalized data were fitted with a shape preserving interpolant line using MATLAB's curve fitting tool. Results of this process are shown in Fig. F.3. Using the curve fitting tool, the value of normalized amplitude at 10 mmHg intervals from 30 - 300 mmHg was determined so that data at the same pressure could be compared for all individuals. A new graph was then produced based on the data obtained from curve fitting, as shown in Fig. F.4. The data from all 10 subjects were combined to determine the mean normalized PPG amplitude for contact pressures ranging from 30 - 300 mmHg in 10 mmHg increments. The mean values were used to construct the final graph shown in Fig. 5.1, and subsequently to determine the optimal contact pressure range.

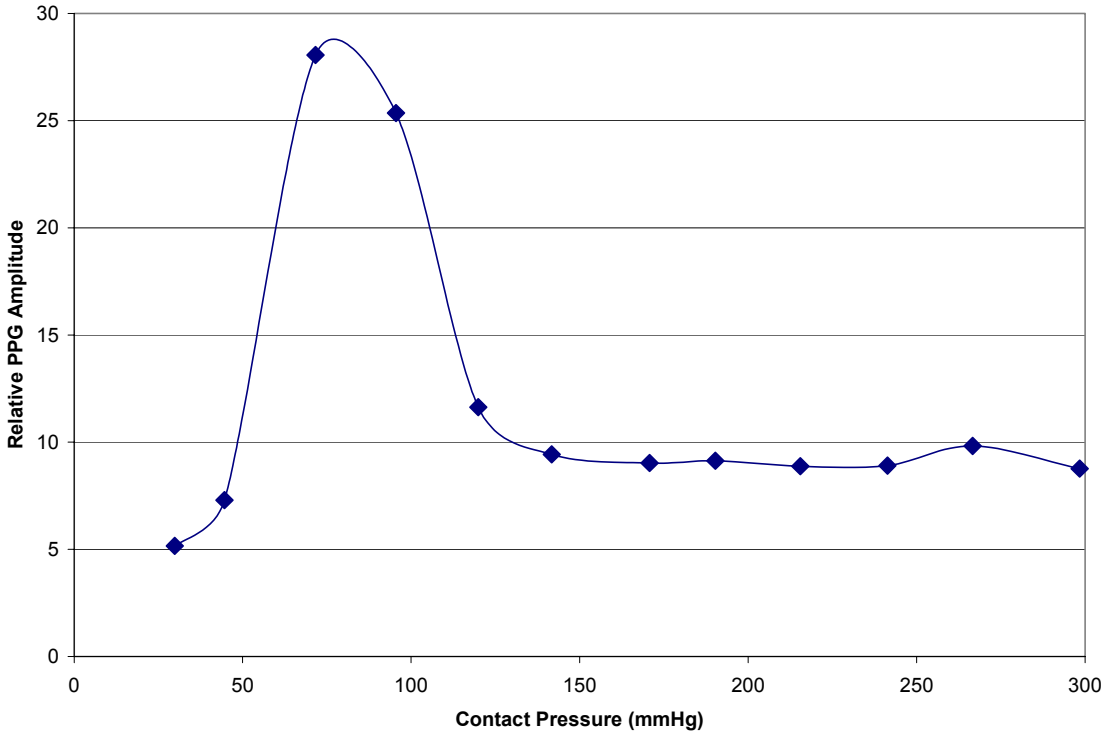

Figure F.1. Typical effects of contact pressure on the relative PPG amplitude from Nonin sensors.

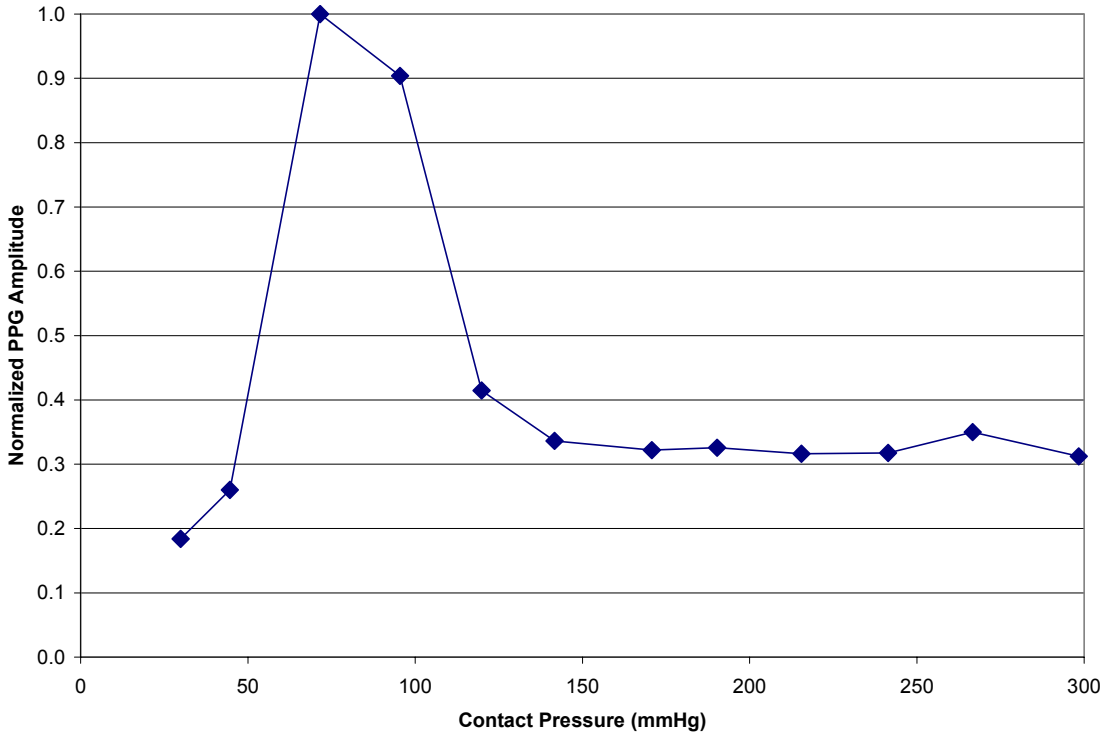

Figure F.2. The effects of contact pressure on the normalized PPG amplitude.

Because measurements were not performed at exactly the same pressure for each individual, the normalized data were fitted with a shape preserving interpolant line using MATLAB's curve fitting tool. Results of this process are shown in Fig. F.3. Using the curve fitting tool, the value of normalized amplitude at 10 mmHg intervals from 30 - 300 mmHg was determined so that data at the same pressure could be compared for all individuals. A new graph was then produced based on the data obtained from curve fitting, as shown in Fig. F.4. The data from all 10 subjects were combined to determine the mean normalized PPG amplitude for contact pressures ranging from 30 - 300 mmHg in 10 mmHg increments. The mean values were used to construct the final graph shown in Fig. 5.1, and subsequently to determine the optimal contact pressure range.

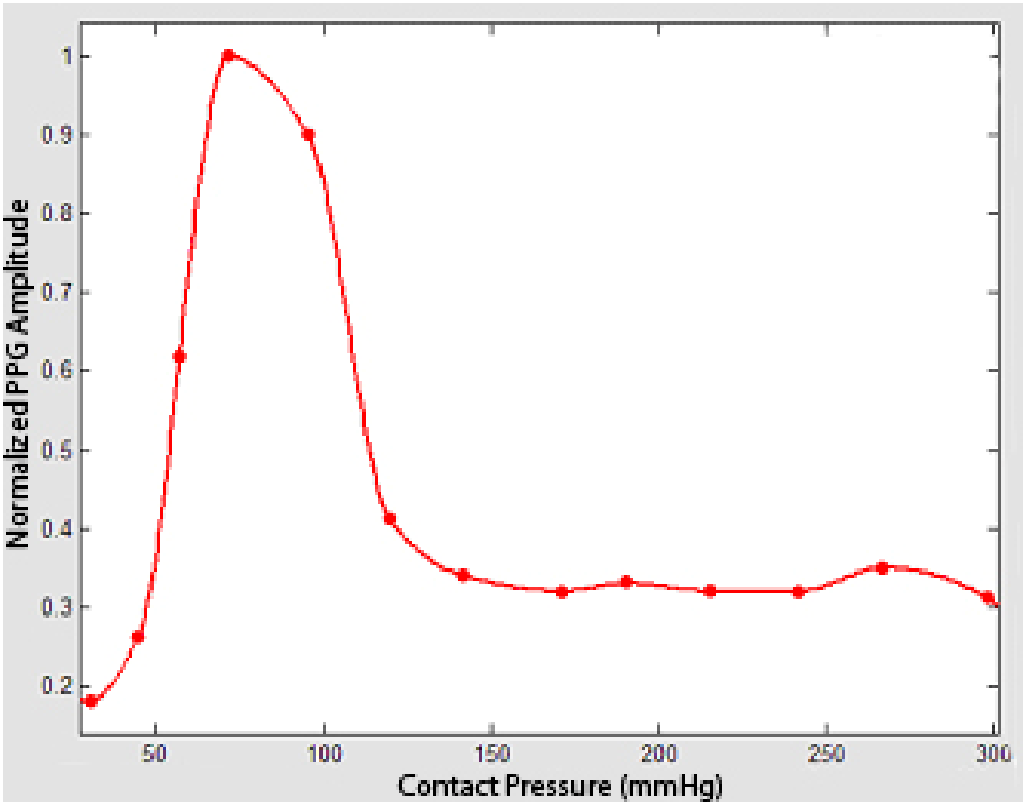

Figure F.3. Shape preserving interpolant fitted line.

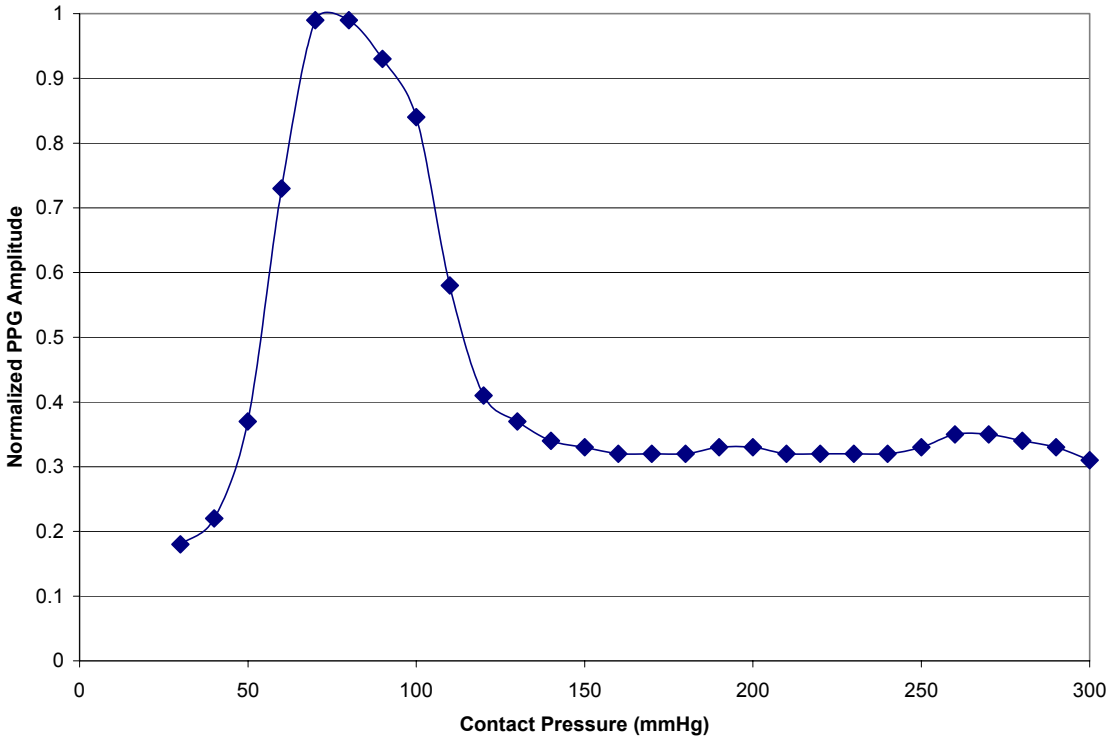

Figure F.4. Measured PPG amplitude normalization and the effects of contact pressure after curve fitting.

Appendix G - Isolating Sensor Housing Design

Two housings were designed for investigation of Specific Aim 2. Each housing consisted of two separate parts fabricated from Delrin®, as shown in Fig. G.1. Although the housings were fabricated to accommodate a Nonin reflectance pulse oximeter sensor, the design can be easily modified for different sensor configurations. Refer to Fig. E.8 and E.9 for the schematic drawings needed to fabricate these parts.

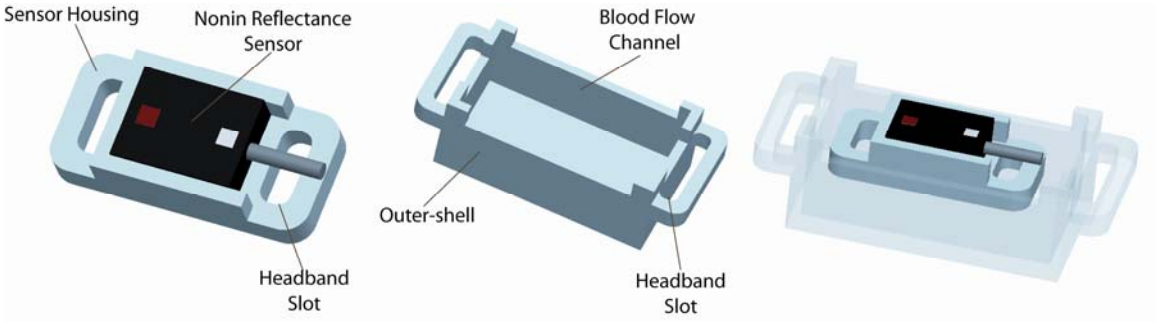

a. **b.** **c.**

Figure G.1. Housing 1 assembly. (a). sensor housing, (b). outer-shell, (c). assembled isolating housing.

Housing 1

The pulse oximeter sensor fits snugly inside the sensor housing as shown in Fig. G.1a. The sensor housing is placed inside the hollow outer-shell (Fig. G.1b), such that it is not in contact with the outer-shell, as shown in Fig. G.1c. Each part is attached to the forehead by means of two individual elastic headbands, as shown in Fig. G.2. Using two bands ensures that each housing remains in intimate contact with the forehead. They also position the sensor housing such that it does not come in contact with the outer-shell. This key concept is what isolates the sensor from pressure disturbances acting on the outer-shell.

The other important feature of this design is the presence of blood flow channels cut into the outer-shell, as shown in Fig. G.1b. For this design, sensor placement is located above the eyebrow as previous studies suggest this is an optimal area for reflectance pulse oximetry at the forehead [56]. Fig. G.3 depicts the arterial and venous network near the eyebrow. This figure shows that the vasculature network runs horizontally and vertically, suggesting the need for blood flow channels on all sides of the outer-shell. In the absence of these blood flow channels, external pressures acting perpendicular to and towards the forehead cause the outer-shell to be displaced into the tissue and may lead to compromised blood flow beneath the sensor. The presence of these blood flow channels helps to maintain normal blood flow to the pulse oximeter sensor if the outer-shell is displaced into the tissue.

Fig. G.5 - G.7 illustrates how pressure disturbances affect the vasculature in the region of the sensor. As can be seen in Fig. G.7 the housing maintains normal blood flow under the sensor in the presence of pressure disturbances. When pressure is applied to the outer-shell, it is displaced into the tissue while the sensor maintains the same contact pressure with the skin. The displacement of the outer-shell into the tissue causes vessel constriction only underneath the four legs of the housing. Therefore, in the presence of pressure disturbances, blood flow to the sensor remains intact. Without blood flow channels, vessel constriction around the perimeter of the outer-shell would reduce blood flow to the sensor, as illustrated in Fig. G.6.

Housing 2

The second housing designed utilizes the same two parts as Housing 1. The difference in this design is the outer-shell which is filled with foam and the sensor housing is sewn to

the foam, thus forming a single hybrid unit, as shown in Fig. E.4. The unit is secured to the forehead by means of an elastic band looped through the outer-shell headband slot.

The functioning of this housing in the presence of pressure disturbances acts in a similar manner as described and illustrated for Housing 1. When pressures that are perpendicular to and acting towards the forehead are applied to the outer-shell, it is displaced into the tissue. At the same time, the foam is compressed, damping the pressure disturbances, thus leaving the sensor unperturbed and in contact with the skin at the same pressure.

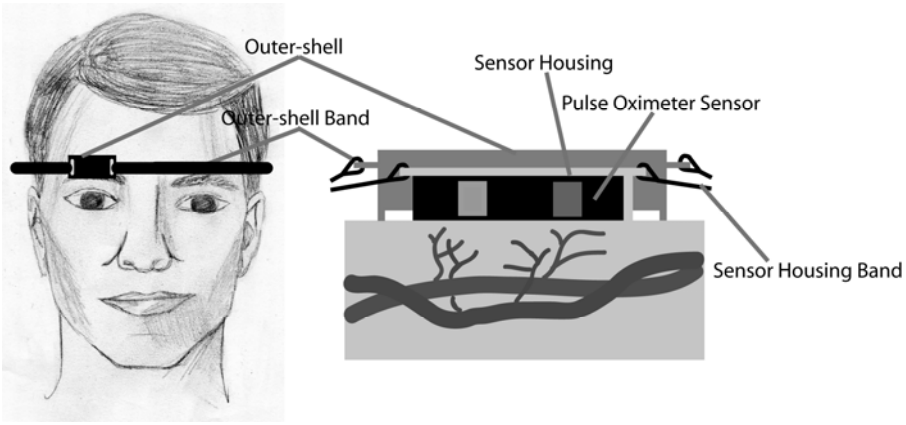

Figure G.2. Attachment of housing to the forehead using elastic headbands [21].

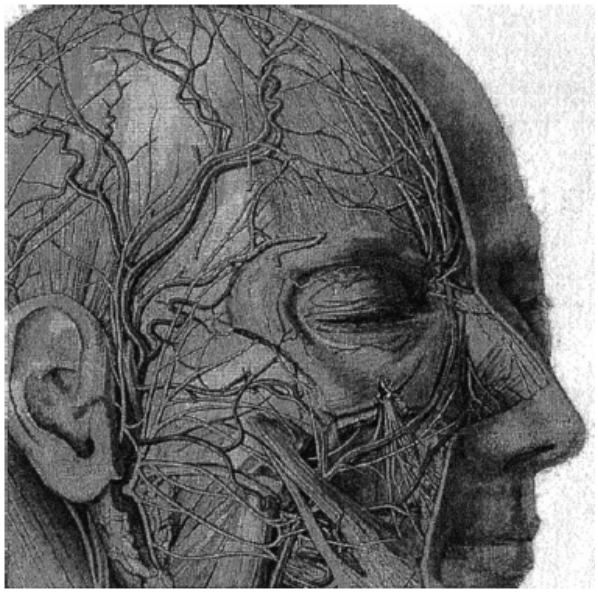

Figure G.3. Arterial and venous network of the head [56].

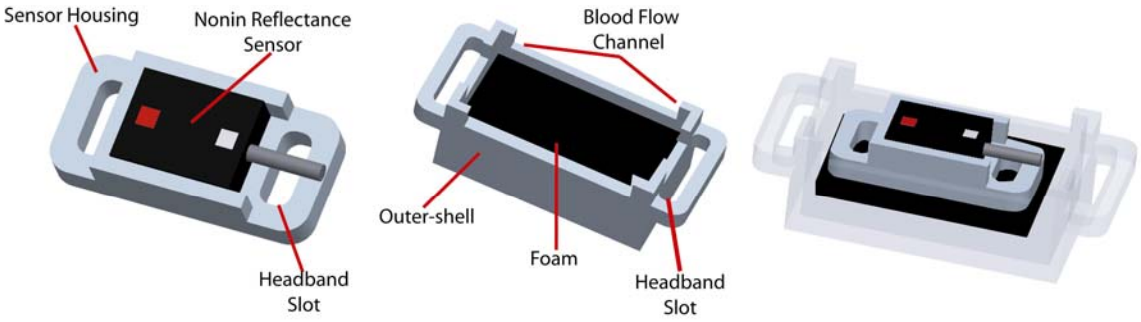

Figure G.4. Housing 2 assembly. (a). sensor housing, (b). outer-shell, (c). assembled isolating housing.

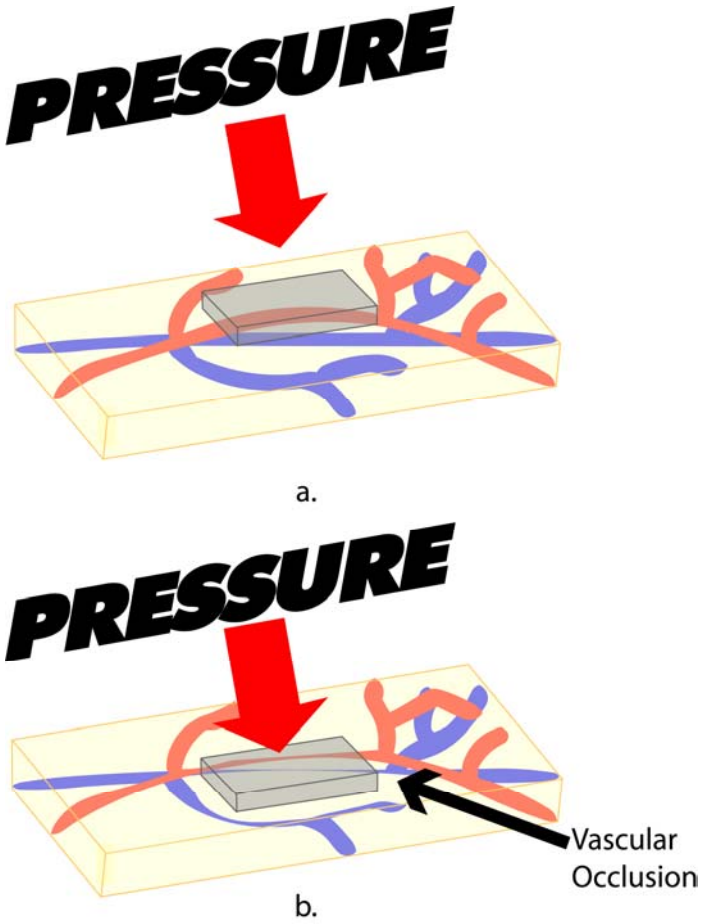

Figure G.5. Pressure disturbance effects on vasculature using current technology. Note vessel occlusion underneath the sensor housing [21]. (a). Before pressure is exerted, (b). Large pressure acting on sensor housing.

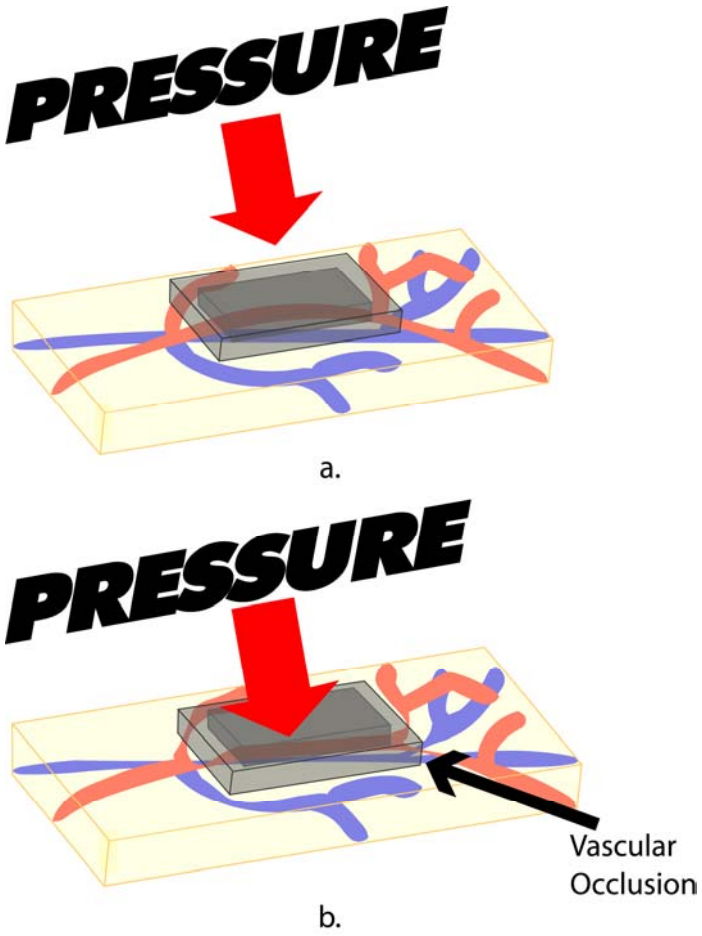

Figure G.6. Pressure disturbance effects on vasculature using designed housing without blood flow channels. Note vessel occlusion at edges of the outer-shell [21]. (a). Before pressure is exerted, (b). Large pressure acting on sensor housing.

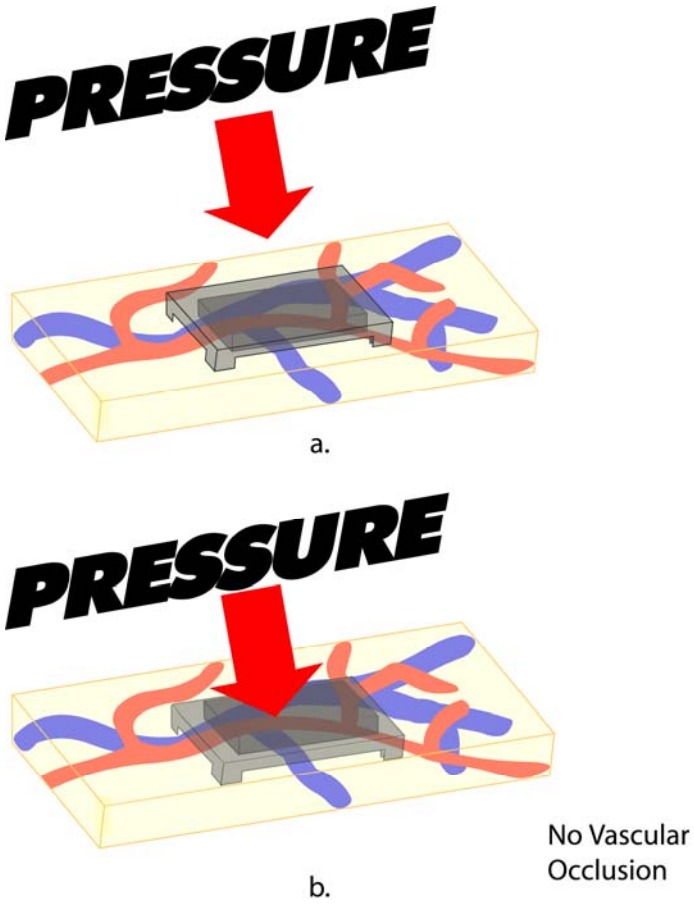

Figure G.7. Pressure disturbance effects on vasculature using designed housing with blood flow channels (minimal constriction) [21]. (a). Before pressure is exerted, (b). Large pressure acting on sensor housing.

For simplicity, only Housing 1 could have been prototyped to study the effects of this concept of pressure artifact reduction as both housings rely on the same principal of isolating the sensor from pressure disturbances. However, Housing 2 is attractive because outfitting the unit to the forehead requires the user to simply place one elastic band around the forehead. On the other hand, Housing 1 requires the user to place two elastic bands around the head and position the two parts correctly. Conversely, the foam can act as a bacteria trap when the unit is worn over extended periods of physical activity. To solve this problem, replacement of the foam with springs was considered. However, this method would be costly when prototyping only a few units.

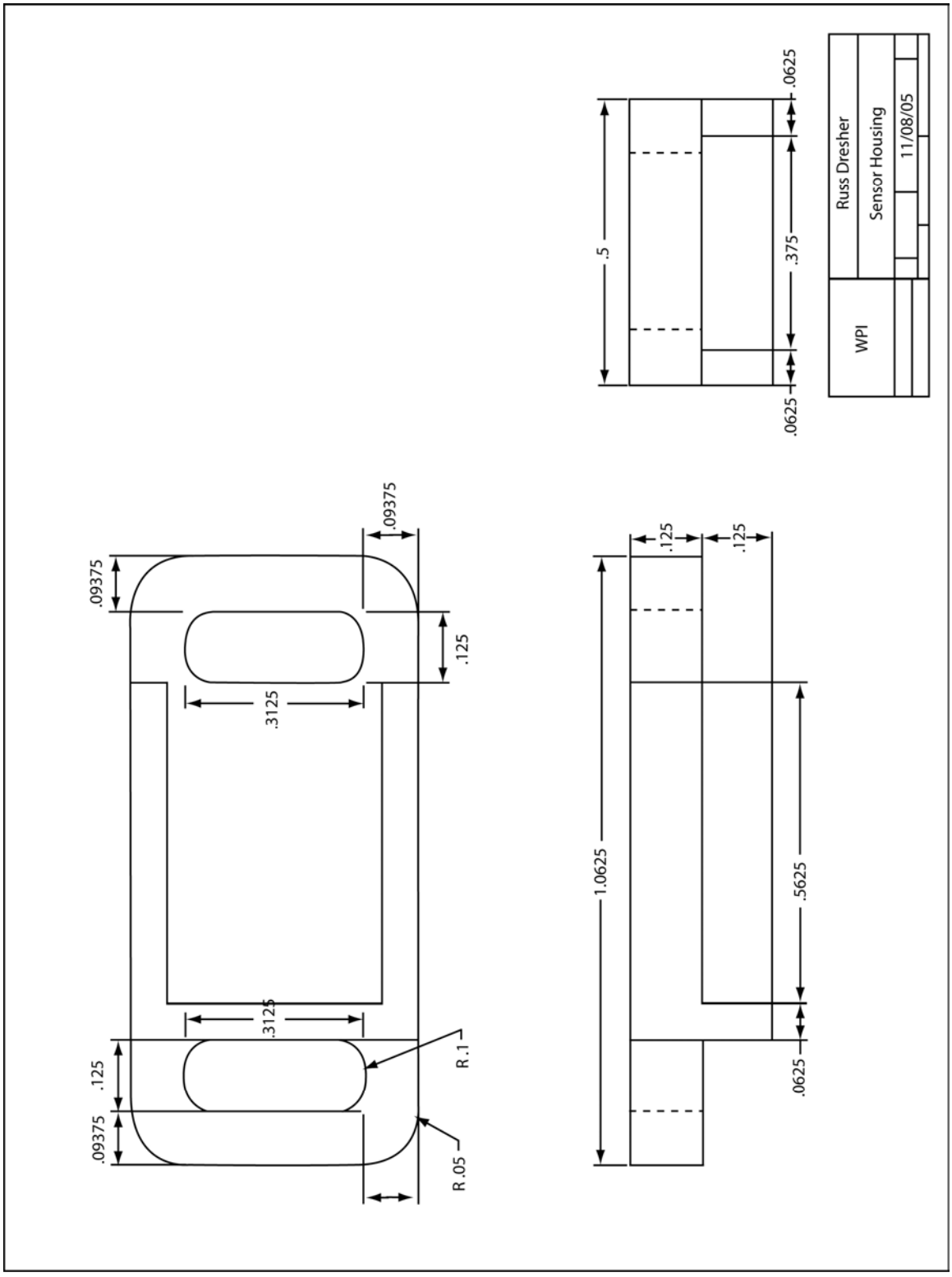

Figure G.8. Sensor housing schematic.

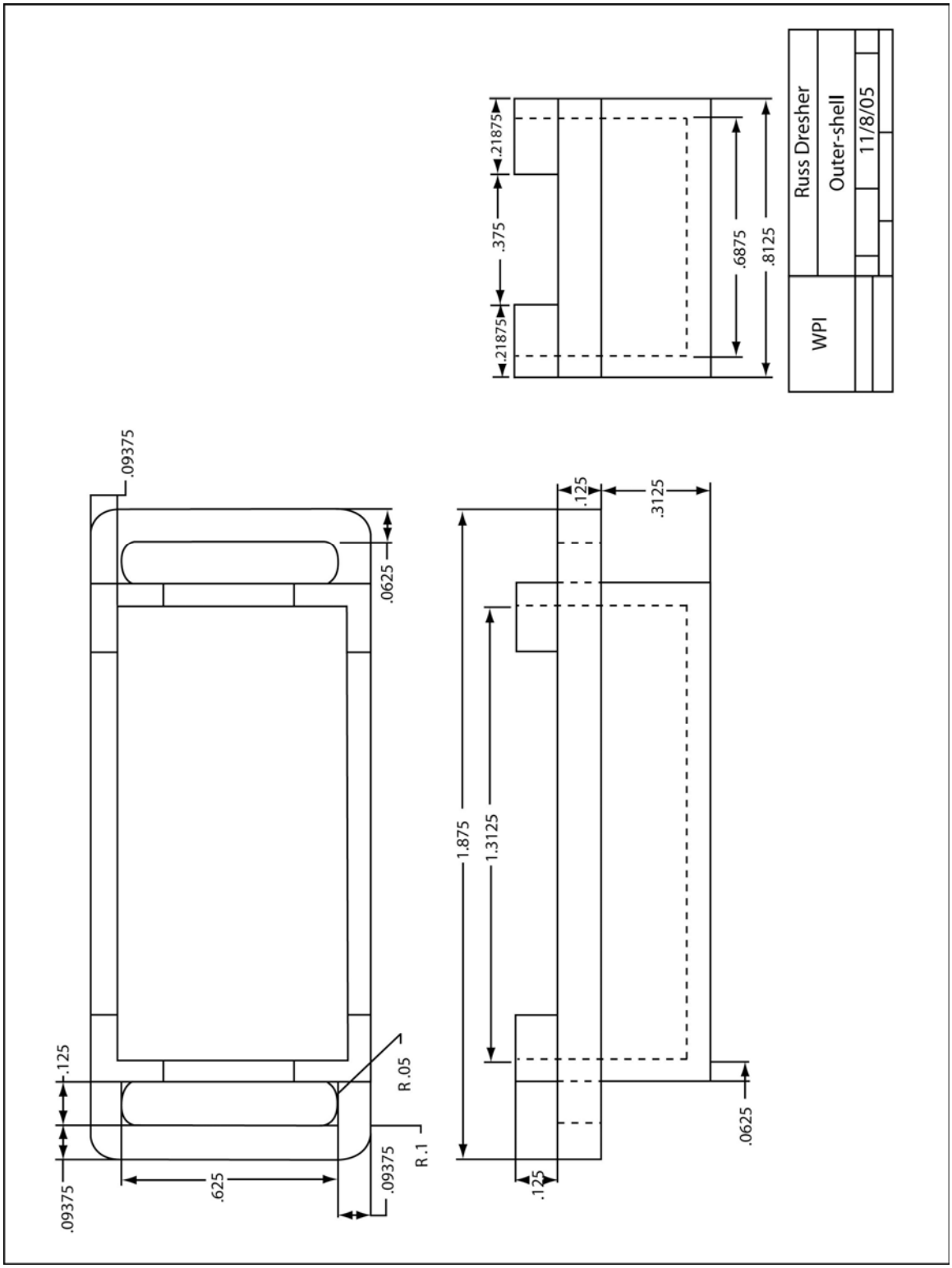

Figure G.9. Outer-shell schematic.